THE JOURNAL OF PHYSICAL CHEMISTRY B

Article

pubs.acs.org/JPCB

# Rationalizing the Catalytic Activity of Copper in the Cycloaddition of Azide and Alkynes (CuAAC) with the Topology of $\nabla^2\rho(r)$ and $\nabla\nabla^2\rho(r)$

Saturnino Calvo-Losada,[†] María Soledad Pino-González,[‡] and José Joaquín Quirante*[,†]

[†]Departamento de Química Física, Facultad de Ciencias, Universidad de Málaga, Campus de Teatinos, s/n. 29071 Málaga, Spain

[‡]Departamento de Química Orgánica, Facultad de Ciencias, Universidad de Málaga, Campus de Teatinos, s/n. 29071 Málaga, Spain

Supporting Information

**ABSTRACT:** The distinct role of the Cu(I) in the Huisgen dipolar cycloaddition of azides to alkynes (denoted as CuAAC) is disclosed by following the evolution of the topology of the Laplacian of the electronic charge density, $\nabla^2\rho(r)$, and its gradient vector field, $\nabla\nabla^2\rho(r)$, along the reaction coordinate with several density functionals (wB97XD, LCwPBE, M06-2X, M06-L, B3LYP) and the 6-311++G(d,p) basis set. Remarkably, in view of the topology of $\nabla^2\rho(r)$ and $\nabla\nabla^2\rho(r)$, the mechanism appears to be diverse (asynchronous concerted or stepwise) depending on the reaction conditions. Overall, the catalyst orchestrates first the formation of the external N−C and subsequently the internal one by following alternatively a pericyclic-like or a pseudopericyclic-like mechanism. The role of the catalyst is envisaged as transforming the type of the mechanism from pericyclic to pseudopericyclic, and thence eventually facilitating the process. The mononuclear process (CuAAC) is concerted (with L = $CH_3CN$) with all the functionals tested (i.e., wB97XD, LCwPBE, M06-2X, M06-L), except for the B3LYP who rendered a stepwise mechanism. Nevertheless, with L = $H_2O$ and $CH_3OH$ attached to the copper, the process becomes asynchronous concerted. Interestingly, upon introduction of the second Cu ($Cu_2$AAC) at our best theory level (i.e., LCwPBE/6-311++G(d,p)), all the processes considered turned out to be concerted except for the 1,4-$Cu_2$AAC which is predicted to be stepwise, with an extremely low enthalpy for the ring-contraction process (0.18 kcal/mol). This fact is explicated by the stability of the intermediate, which is in turn rationalized by the hole within the valence shell of the carbon attached to the Cu and the position of the $(3,-3)_{LP}$, of the internal N, toward it. Furthermore, due to the tiny energy difference between the stepwise dinuclear and concerted mononuclear mechanisms (0.39 kcal/mol), we argue that the concurrence of both processes (CuAAC and $Cu_2$AAC) is feasible.

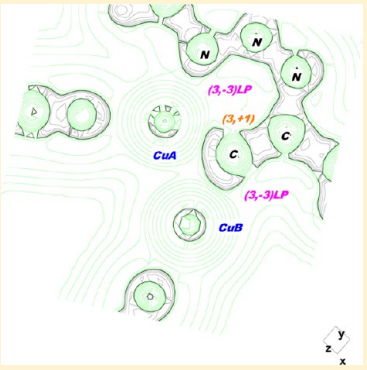


## INTRODUCTION

The copper-catalyzed version of the Huisgen 1,3 dipolar cycloaddition between azides and alkynes (dubbed as CuAAC)[1−13] represents the premier example of the so-called "click chemistry".[1] Relevant features of this reaction are: it is virtually quantitative, it has a high regioselectivity, it is insensitive to reaction conditions, and organic or even aqueous solvents are possible.[1,3,11] Nonetheless, it is limited to terminal alkynes.[1,2,4−8] In spite of its importance, many aspects of its mechanism remain unclear,[1,6,7] such as the role of the solvent,[2,11−13] the regioselectivity of the process,[7] the oxidation state of the Cu involved,[8] the number of Cu atoms that participate in the catalysis,[1,9] the influence of ligands,[10,11] or the distinct role of the copper as opposed to other catalysts.[1,7,11]

The first mechanistic proposal (outlined in Scheme 1),[3,5] subsequently confirmed theoretically with the B3LYP[14−16] density functional (DF),[17] involved only one Cu atom and was considered to begin with the formation of an acetylide preassociation complex by the coordination of the azide to the Cu(I) and to progress by a stepwise mechanism through a six-membered metallacycle intermediate which leads eventually to a triazole with a "negligible" energy barrier (see Scheme 1).[5] Strikingly, with L = $H_2O$, the method predicted an energy barrier around 3 kcal/mol, whereas for L = $CH_3CN$ the energy barrier amounted to an unexpected negative value (−0.2 kcal/mol).[5] These authors attributed the latter to drawbacks in the DFT method and, notwithstanding, they concluded that the process ran in a stepwise manner.[5] Subsequent kinetic studies by Rodionov et al. found an experimental second-order kinetics for the Cu concentration under catalytic conditions,[9] and arrived at the conclusion that the simplest explanation was the probable participation of multinuclear clusters of Cu(I).[9] B3LYP calculations[18−20] supported this hypothesis, and very recently, Worrell et al. designed an *ad hoc* experiment that confirmed the participation of dinuclear clusters of Cu in the process.[21]

In order to design novel synthetic routes with azides by using carbohydrates,[22−24] we have started off a research line aimed at comprehending the subtleties of the process. To this end, we have applied the analysis of the topology $\nabla^2\rho(r)$ and $\nabla\nabla^2\rho(r)$ in the context of the QTAIM[25] that has proven crucial in discerning between pseudopericyclic[26] and pericyclic mechanisms (see Scheme S1).[27,28]

**Received:** June 4, 2014
**Revised:** November 27, 2014
**Published:** December 9, 2014





DOI: 10.1021/jp5055414
J. Phys. Chem. B 2015, 119, 1243−1258

**Scheme 1. Concerted and Stepwise Mechanisms for the Mononuclear and Dinuclear Catalyzed "Click" Reaction with Cu(I) and for the Huisgen Reaction[a]**

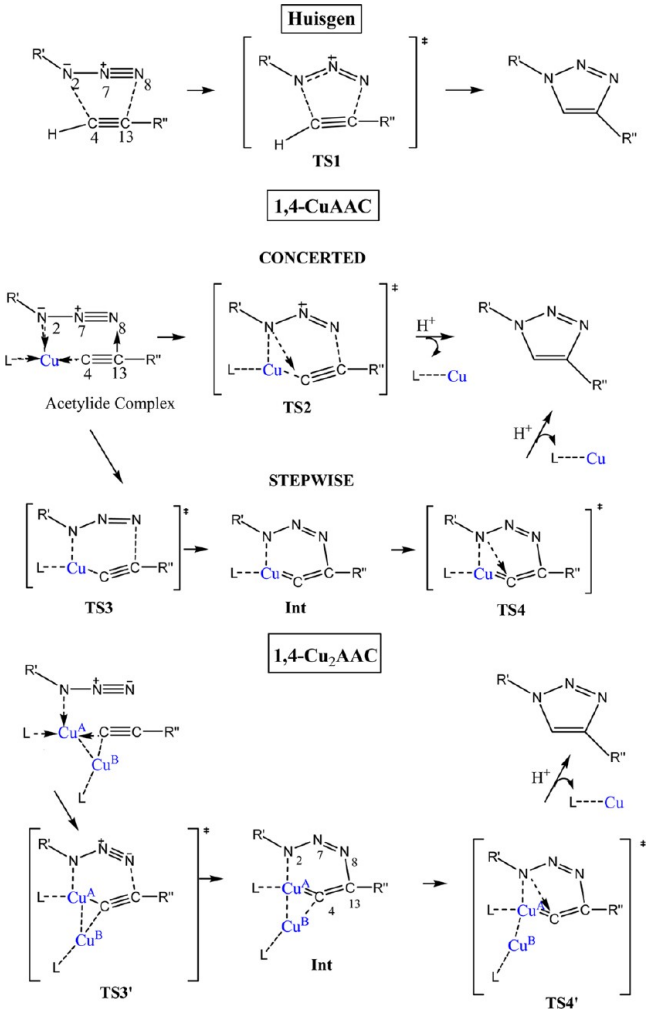


[a]R′, R″ = $CH_3$ and L = $CH_3CN$, $H_2O$, or $CH_3OH$. The atom numbering used in the calculations is outlined.

On the basis of the study of a plethora of pericyclic and pseudopericyclic processes, we have found distinct topological features between pericyclic and pseudopericyclic[27,28] modes of reaction that could be added to that proposed by Birney some time ago.[29] In particular, for the pseudopericyclic processes, an atom acts as a base donating charge concentration (CC) toward an acid given by a hole (charge depletion, CD) in the valence shell of the electrophilic atom from the very beginning of the process. The very power of the topology of $\nabla^2\rho(\mathbf{r})$ is manifested in that several CC (given by its critical points) can occur and hence it is not restricted to "entire" electronic lone pairs in the sense of Lewis. As a matter of fact, three types of pseudopericyclic mechanisms have been identified so far (see Scheme S1, Supporting Information), depending on the type of charge concentration posited by the nucleophile and the electrophile.[28] Remarkably, this type of "pseudopericyclic contact"[27,28,30] keeps the adducts linked from the very beginning of the process, and as long as the nucleophile approaches the hole, the latter becomes enlarged.[28,30] In contradistinction, for the pericyclic process, both atoms cooperate in the bond formation by displacing charge density from a conjugate $\pi$ bond and accumulating it on terminal atoms (see Scheme S1, Supporting Information). The larger energy barrier can be explicated by the great electronic reorganization the molecule must carry out to move density toward the terminal atoms. Precisely, we will rationalize the different versions of the CuAAC as the interplay between pericyclic and pseudopericyclic alternatives as caused by the catalyst but with a remarkable novelty: the pseudopericyclic contact encompasses a carbon atom as playing the role of the nucleophile (see below).

Regarding the title reaction, first we have dealt with the regioselectivity of the process by comparing the 1,4- and 1,5-CuAAC mechanisms (visualized by the transformation of the atomic graphs given by $\nabla\nabla^2\rho(\mathbf{r})$) and arrived at the interesting conclusion that for each route the mechanism was diverse.[30] In this paper, in order to gain insight into the catalytic activity of copper, we will compare the evolution of the topology of $\nabla^2\rho(\mathbf{r})$ and $\nabla\nabla^2\rho(\mathbf{r})$ along the reaction coordinate for the simplest mononuclear 1,4-CuAAC and dinuclear 1,4-$Cu_2$AAC with the noncatalyzed counterpart with R′ = R″ = $CH_3$ and L = $CH_3CN$, $H_2O$, $CH_3OH$ (see Scheme 1). As a matter of fact, as it did occur for the 1,5-CuAAC the topology of $\nabla^2\rho(\mathbf{r})$ and $\nabla\nabla^2\rho(\mathbf{r})$ for the mononuclear mechanism is modified by the inclusion of the second Cu atom. Given the tiny difference in the enthalpies, we contend that the process could follow a "concerted" (1,4-CuAAC) or a "stepwise" (1,4-$Cu_2$AAC) mechanism, or even both types of mechanisms, depending on the reaction conditions. This situation resembles that described by Jencks[31,32] and Young[33] some time ago concerning $SN_2$ reactions, where the process passed from concerted to stepwise fashion depending on the stability of the carbocation intermediate.[31,32] However, to our knowledge, no similar situation has been reported before for transition metals. The regioselectivity of the dinuclear process and the influence of the counterion in the mechanism will be discussed elsewhere.

## QUANTUM TOPOLOGICAL METHODS

In the QTAIM,[25] the reactivity of the molecules is reflected in the topology of the Laplacian of the charge density,[34] $\nabla^2\rho(\mathbf{r})$, for its appearance in the local virial theorem relating locally the kinetic and potential densities for a stationary state ($(\hbar^2/4m)\nabla^2\rho(\mathbf{r}) = V(\mathbf{r}) + 2G(\mathbf{r})$).[35] Thereby, it highlights where the charge density is preferentially concentrated ($\nabla^2\rho(\mathbf{r}) < 0$), hence dominating $V(\mathbf{r})$, and depleted ($\nabla^2\rho(\mathbf{r}) > 0$), thus dominating $G(\mathbf{r})$ instead.[36−39] The structure of an atom is reflected in the alternation of shells of charge concentration (CC) with $\nabla^2\rho(\mathbf{r}) < 0$ and charge depletion (CD) with $\nabla^2\rho(\mathbf{r}) > 0$ up to the 4 period.[40−42] With the last shell being crucial for chemistry, the so-called valence shell of charge concentration (VSCC) and its associated charge depletion (VSCD).[37,38]

Critical points (CPs)[25,36−39,43] of $L(\mathbf{r}) = -\nabla^2\rho(\mathbf{r})$ are characterized in the QTAIM by a pair of numbers $(\omega, \sigma)$: the rank, $\omega$, is equal to the number of nonzero eigenvalues of the Hessian matrix of $\nabla^2\rho(\mathbf{r})$, and the signature, $\sigma$, indicates the algebraic sum of the signs of the eigenvalues.[25] They are nonbonded and bonded local maxima given by $(3,-3)$ CPs, local saddle given by $(3,+1)$ CPs and $(3,-1)$ CPs, and local minima given by $(3,+3)$ CPs. Note that bonded $(3,-3)$ CPs, denoted as $(3,-3)_{BP}$, and nonbonded $(3,-3)$ CPs, denoted as $(3,-3)_{LP}$ CPs are topologically but not chemically equivalent. Precisely, the nonbonded maxima of $L(\mathbf{r})$ determine the *nucleophilic sites* and the $(3,-3)_{BP}$ appear within the basin of the bonding atom. On the other side, the *electrophilic sites* are determined by the "holes" within the VSCC, as given by $(3,+1)$


DOI: 10.1021/jp5055414
J. Phys. Chem. B 2015, 119, 1243−1258

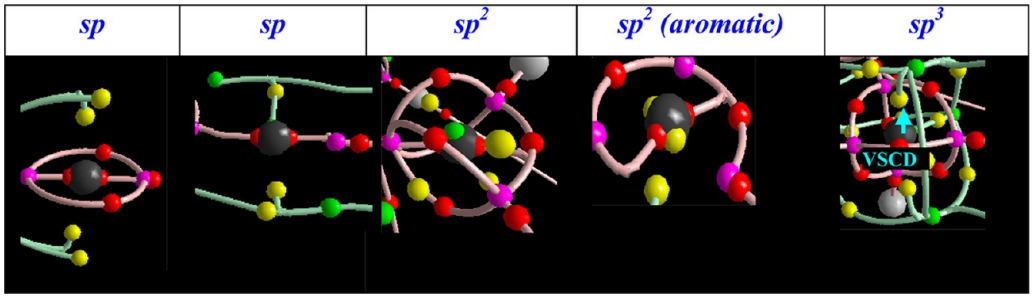


**Figure 1.** Atomic graphs associated with the VSCC of typical C atoms. Purple points are maxima $(3,-3)_{BP}$ and represent the *vertices* of the "graph", red points stand for $(3,-1)$ CPs and define the *edges*, and yellow points stand for $(3,+1)$ CPs and define the *faces* of the "graph". $(3,+3)$ CPs minima face off $(3,+1)$ CPs in the complementary VSCD.

CPs (note that $(3,+3)$ CPs cannot be located within the VSCC). Interestingly, to fullfill the aforementioned local virial theorem, in the course of a reaction, $(3,-3)_{LP}$ CPs will be driven to "reach" minima in $L(\boldsymbol{r})$. This statement has been called the Laplacian complementarity principle,[44] and represents a extension of the Lewis acid−base theory.[25,39,44] Despite its direct relation with reactivity, theoretical studies utilizing the topology of $\nabla^2\rho(\boldsymbol{r})$ in the last 25 years have been scarce,[45−51] probably due to its inherent complexity.[37] Nonetheless, it has been utilized to account for the geometry of several metal and transition metal compounds[52−61] and crystals[62] and more importantly has provided a physical basis to the VSEPR theory of Gillespie.[52−54,63−66] Its homeomorphic nature has been shown with the electronic localization function (ELF),[67] albeit the former surpasses the latter for it is not a "truncated function".[68]

On the other hand, the gradient of the Laplacian distribution, the $\nabla\nabla^2\rho(\boldsymbol{r})$ vector field which provides the direction of variation of the charge density accumulation, has not been so fully explored. The gradient trajectories connect CPs of $L(\boldsymbol{r}) = -\nabla^2\rho(\boldsymbol{r})$ of the valence shell of charge concentration (VSCC), defining the atomic graph[25,37,38,55] of an atom. This graph[69] would include bonded $(3,-3)$ CPs (denoted as $(3,-3)_{BP}$) as vertices, $(3,-1)$ CPs as edges, and (3,+1) CPs as faces.[70] Popelier et al. defined planar graphs based on the CPs of the $L(\boldsymbol{r})$ except for $(3,+1)$, not accounting so for the electrophilic sites.[43] Depending on the different molecular environments, each atom can adopt an atomic graph corresponding to its hybridization pattern (see Figure 1).[28,59]

For well-behaved functions (Morse functions),[71] CPs are isolated. Unfortunately, during the chemical process, as we will see, degenerate CPs (non-Morse function) appear given that atoms are unbounded open systems, as has been shown for the gradient vector field of $\rho(\boldsymbol{r})$,[25] some lines will escape to infinity[43,72] emanating from $(3,-3)_{LP}$ CPs and also from $\pi$ multiple bonds signaling possible nucleophilic activity. In addition, for a gradient field, the gradient trajectories only cross at CPs.[73] Notwithstanding, during chemical processes, the atomic graphs are modified and hence new CPs are created or modified. Crossing of gradient lines will appear, signaling a singularity[73] in the gradient field and anticipating the creation of a new CP in the $\nabla^2\rho(\boldsymbol{r})$ manifold.

In pseudopericyclic reactions, we have found out that usually each atom will tend to decrease the size of the holes by increasing the number of $(3,-3)$ CPs, thus augmenting the faces of the associated polyhedron, or by adopting an "aromatic-type" atomic graph (i.e., without $(3,+1)$ CPs above and below the molecular plane, see Figure 1). This would entail a lower reactivity and consequently an increase in local hardness, eventually fulfilling a local version of the maximum hardness principle.[74]

Remarkably, closed-shell and covalent interactions[25] are clearly discerned and further characterized with the topology of $\nabla\nabla^2\rho(\boldsymbol{r})$. The former exhibit either a gradient trajectory emerging from a $(3,-3)_{LP}$ directed at a $(3,+1)$ CP[75] or both gradient trajectories converging with each other. When a covalent bond is formed, they would collapse eventually yielding a $(3,-3)_{BP}-(3,-1)-(3,-3)_{BP}$ triplet of CPs.[28,58,60]

Further, given that "many results indicate that the reactivity of most types of organic molecules depends upon the relative stereochemistry of particular electron pairs, bonded and nonbonded, as stated by Deslongchamps,[76] we think that the Laplacian of the charge density—as providing a mapping of the $(3,-3)_{LP}$ and $(3,-3)_{BP}$—along with the trajectories of $\nabla^2\rho(\boldsymbol{r})$—providing the directionality of change—could account for the stereoelectronic effects proposed by Deslongchamps[76] in general fashion.

For transition metals (up to 4 period), the Laplacian exhibits an outer depletion shell (VSCD) that coordinates ligands through donor−acceptor (D → A) or dative interactions.[55−61] Hence, it provides a topological definition of the coordinate bond:[77] a $(3,-3)_{LP}$ of the donor appears aligned toward a $(3,+1)$ CP or a $(3,+3)$ CP in the acceptor.[55−61]

## COMPUTATIONAL DETAILS

The dubious results of Himo et al.[5] prompted us to carry out a DFT study[30] to assess the reliability of the B3LYP[14] DF by using alternative functionals such as LCwPBE,[78,79] M06-2X,[80] M06-L,[80] and wB97XD[81] recently tested.[82] Two comprehensive reviews have also been very recently reported by Tsipis.[83,84] For comparison, the uncatalyzed version was studied with the LCwPBE functional, for it rendered the most consistent description. All the calculations were carried out with the G09 and G09w suites of programs.[85] Optimizations with all the DFs and Pople's 6-311++G(d,p) basis set were performed in solution with the analytic Hessian computed at every step at the same levels of theory. The transition structures (TSs) were confirmed by frequency calculations and subsequent inspection of the normal modes with the GaussView 5.0 program.[86] Unfortunately, for the dinuclear vdW complex and the intermediate, only the first two convergence criteria were achieved. The solvent effects were introduced with the PCM method developed by Tomasi et al.[87] and implemented in G09, taking $H_2O$, $CH_3OH$, and $CH_3CN$ as solvents. It should be mentioned that the introduction of the solvent was crucial to achieve convergence in some TSs. To mimic the mixture of solvents of


DOI: 10.1021/jp5055414
J. Phys. Chem. B 2015, 119, 1243−1258

**Chart 1. Energy Profiles for the (A) Mononuclear 1,4-CuAAC, (B) 1,3-Huisgen, and (C) Dinuclear 1,4-$Cu_2$AAC, in Water and with L = $CH_3CN$ at Different Theory Levels with the 6-311++G(d,p) Basis Set[a]**

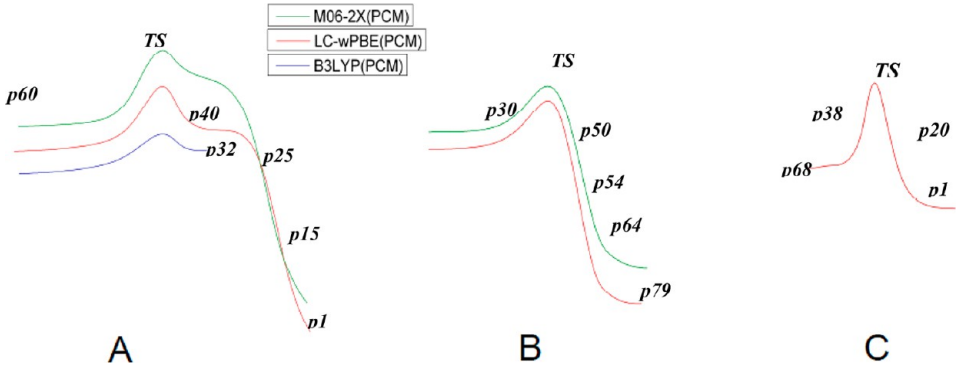


[a]Selected points from the IRCs, to be analyzed afterwards, are indicated.

the experimental conditions (for instance, of acetonitrile and water[2]), several solvents and ligands were combined. The connection of the TS with minima was confirmed with the new IRC algorithm[88] implemented in G09, with 50 points in each direction and computing the analytic Hessian at every step at the same levels of theory. The topology of the electronic charge density $\rho(\boldsymbol{r})$, the Laplacian $\nabla^2\rho(\boldsymbol{r})$, their respective gradient vector fields $\nabla\rho(\boldsymbol{r})$ and $\nabla\nabla^2\rho(\boldsymbol{r})$, the localization $\lambda$, and delocalization indices $\delta(X,Y)$,[25,89] were analyzed with the AIM2000 v.2[90] program with wave functions (wfn's) built up with the selected DFs and 6-311++G(2d,2p) and 6-311++G(3d,p) basis sets for the catalyzed (CuAAC and $Cu_2$AAC) and Huisgen, respectively. The electronic localization function (ELF)[91] and non-covalent interaction (NCI)[92] surfaces, were generated with Gabedit (v. 2.4.8) software.[93] To assess the reliability of the monodeterminantal description, the *T1diag* proposed by Lee et al. was computed at CCSD/6-31G(d) for the basic system[94] and rendered a value below the cut-value of 0.02 proposed by them, supporting the use of a monodeterminantal wfn for the Huisgen. The stability of the wave functions was also assessed by the algorithm implemented in G09.[95] The natural molecular orbitals (MOs) were generated at LCwPBE/6-31G(d) from geometries at LCwPBE/6-311++G(d,p).[96]

## RESULTS

**Energetics.** Chart 1 shows the energy profiles from the acetylide complex to the five-membered metallacycle computed at the M06-2X(PCM)/6-311++G(d,p), B3LYP(PCM)/6-311++G(d,p) and LCwPBE(PCM)/6-311++G(d,p) theory levels for the 1,4-CuAAC (entry A), M06-2X(PCM)/6-311++G(d,p), and LCwPBE(PCM)/6-311++G(d,p) levels for the Huisgen (entry B) and at the LCwPBE(PCM))/6-311++G(d,p) theoretical level for the 1,4-$Cu_2$AAC (entry C). Unfortunately, the wB97XD IRC was obtained only in one direction and M06-L exhibited problems of convergence, so they will not be commented on.

Selected points to be topologically analyzed after being picked up from the respective IRC, computed at LCwPBE/6-311++G(d,p), are indicated in the energy profiles. In particular, for 1,4-CuAAC (Chart 1, entry A): ***p60***, **TS2**(***p51***), ***p40***, ***p32***, ***p25***, ***p15***, and ***p1***; for Huisgen (Chart 1, entry B): ***p30***, **TS1**(***p46***), ***p50***, ***p54***, ***p64***, and ***p79***; and for 1,4-$Cu_2$AAC (Chart 1, entry C): ***p68***, ***p38***, **TS3′**, ***p20***, and ***p1***. For all the systems, the initial reactants would also be considered. Besides, for the 1,4-$Cu_2$AAC, the intermediate (***Int***) and the TS (***TS4′***) that connects it with the triazole will also be studied. The corresponding molecular graphs derived from the CPs of $\rho(\boldsymbol{r})$ and trajectories of $\nabla\rho(\boldsymbol{r})$ are depicted in Figure 2, and the corresponding geometries are plotted in Figure S2 (Supporting Information).

As can be seen in Figure 2, the neutral species exhibits trigonal geometry for the acetylide complex (see also Figures S1 and S2, Supporting Information). Although Cu(I) usually yields tetrahedral complexes, some planar trigonal ones have also been experimentally reported.[66,77] Remarkably, when L = $CH_3CN$ (in water and acetonitrile), all the DFs except for the B3LYP predict a straight asynchronous concerted process connecting the acetylide complex to the five-membered metallacycle through TS2 (see Scheme 1) without the participation of the six-membered metallacycle intermediate. Therefore, for this case, the ring contraction of the six-membered ring to yield the triazole (points ***p40*** to ca. ***p25*** on the IRC) is accomplished without energy demand. On the contrary, when L = $H_2O$ or $CH_3OH$ (solvent $H_2O$, $CH_3OH$), LC-wPBE and wB97XD DFs predict a stepwise process. As a consequence, the electronic nature of the ligands stabilizing the Cu(I) appears to be crucial in the nature of the CuAAC mechanism.[29] With two copper atoms, the ***TS4′*** was located with M06-2X and LCwPBE DFs. Unfortunately, the IRC departing from ***TS4′***, which connects the latter with the five-membered ring, aborted for the LCwPBE DF, probably due to the flatness of the potential energy surface (PES).

The activation entalphies computed from the initial van der Waals (vdW) complexes at LCwPBE/6-311++G(d,p) amount to 25.34, 18.82, and 18.43 kcal/mol for the Huisgen, 1,4-CuAAC, and 1,4-$Cu_2$AAC, respectively. The latter figures are close to that predicted for intermediate pseudopericyclic processes.[27,28] In view of the tiny difference between mononuclear and dinuclear ligation (about 0.39 kcal/mol), the concurrence of the 1,4-CuAAC and 1,4-$Cu_2$AAC should not be discarded *a priori*. Furthermore, this could explain the participation of the two coppers in the mechanism suggested by Worrell et al.[21] In this regard, the stability of the intermediate, the formation of the acetylide complex, and the nature of the copper counterion[1] could also be determinant. At the moment, the inclusion of a chloride attached to a second copper does not modify the stepwise nature of the process; nonetheless, more computations are being conducted to clarify this point. The activation enthalpy for the contraction of the ring (see Scheme


DOI: 10.1021/jp5055414
J. Phys. Chem. B 2015, 119, 1243−1258

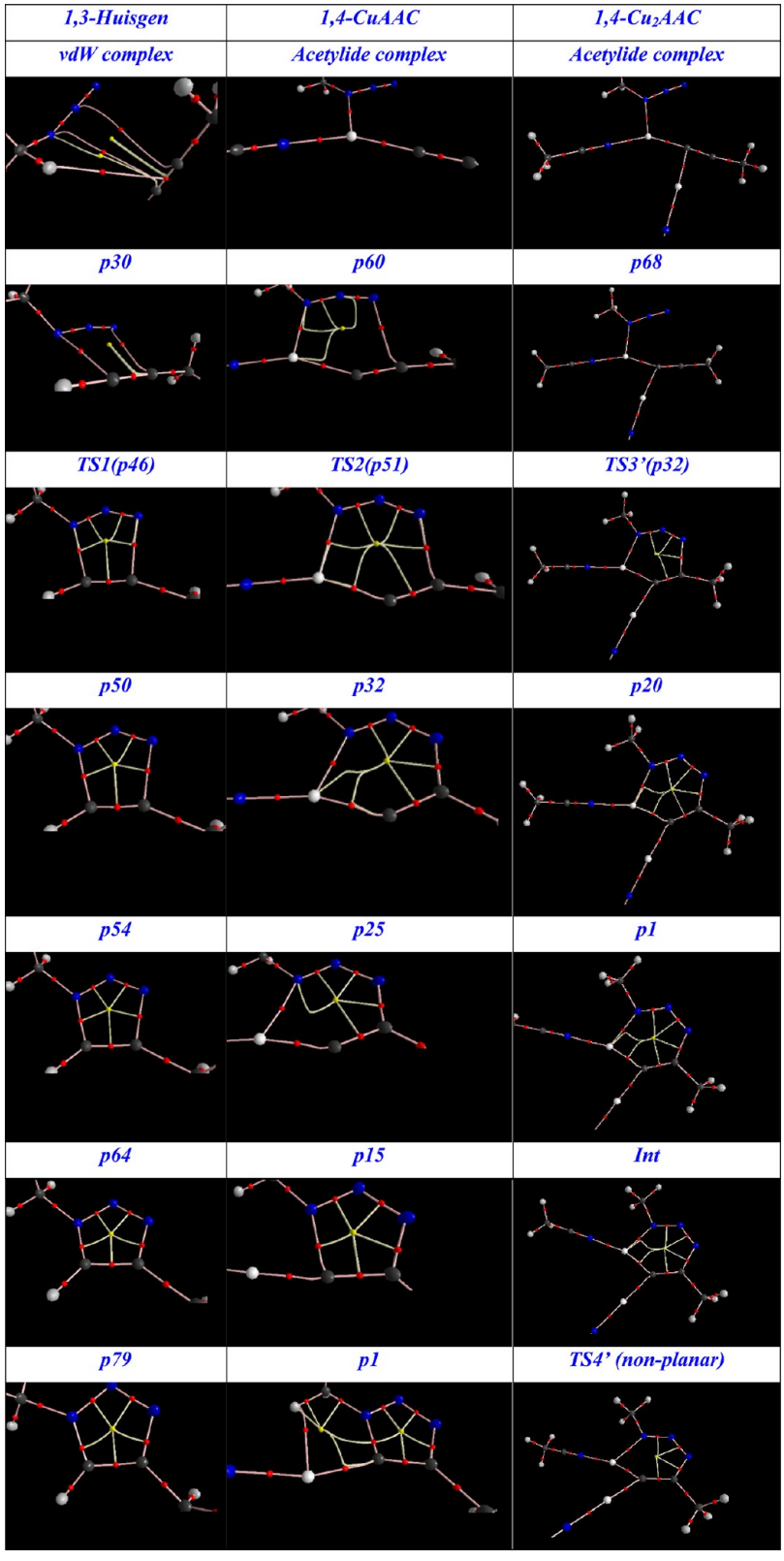


**Figure 2.** Molecular graphs of selected structures along the IRC for the Huisgen (left), 1,4-CuAAC (middle), and 1,4-$Cu_2$AAC (right) processes as derived from trajectories of $\nabla\rho(\boldsymbol{r})$. (3, −1) CPs are plotted in red and (3, +1) CPs in yellow. The number in parentheses corresponds to the point in the IRC. For the *p1* of 1,4-$Cu_2$AAC, an anomalous (3, −1) CP was located (not shown).

1) amounts to only 0.18 kcal/mol at LCwPBE/6-311++G(d,p); therefore, the process appears to be a very facile one. To locate the associated TS on the PES, the inclusion of the solvent turned out to be determinant.

As expected, the B3LYP DF does not reproduce the vdW interactions in the initial acetylide complex for the 1,4-CuAAC, and predicts the N2 and Cu to be 4.79 Å far apart as opposed to the 2.24 and 2.41 Å predicted with LC-wPBE and wB97XD



DOI: 10.1021/jp5055414
*J. Phys. Chem. B* 2015, 119, 1243−1258

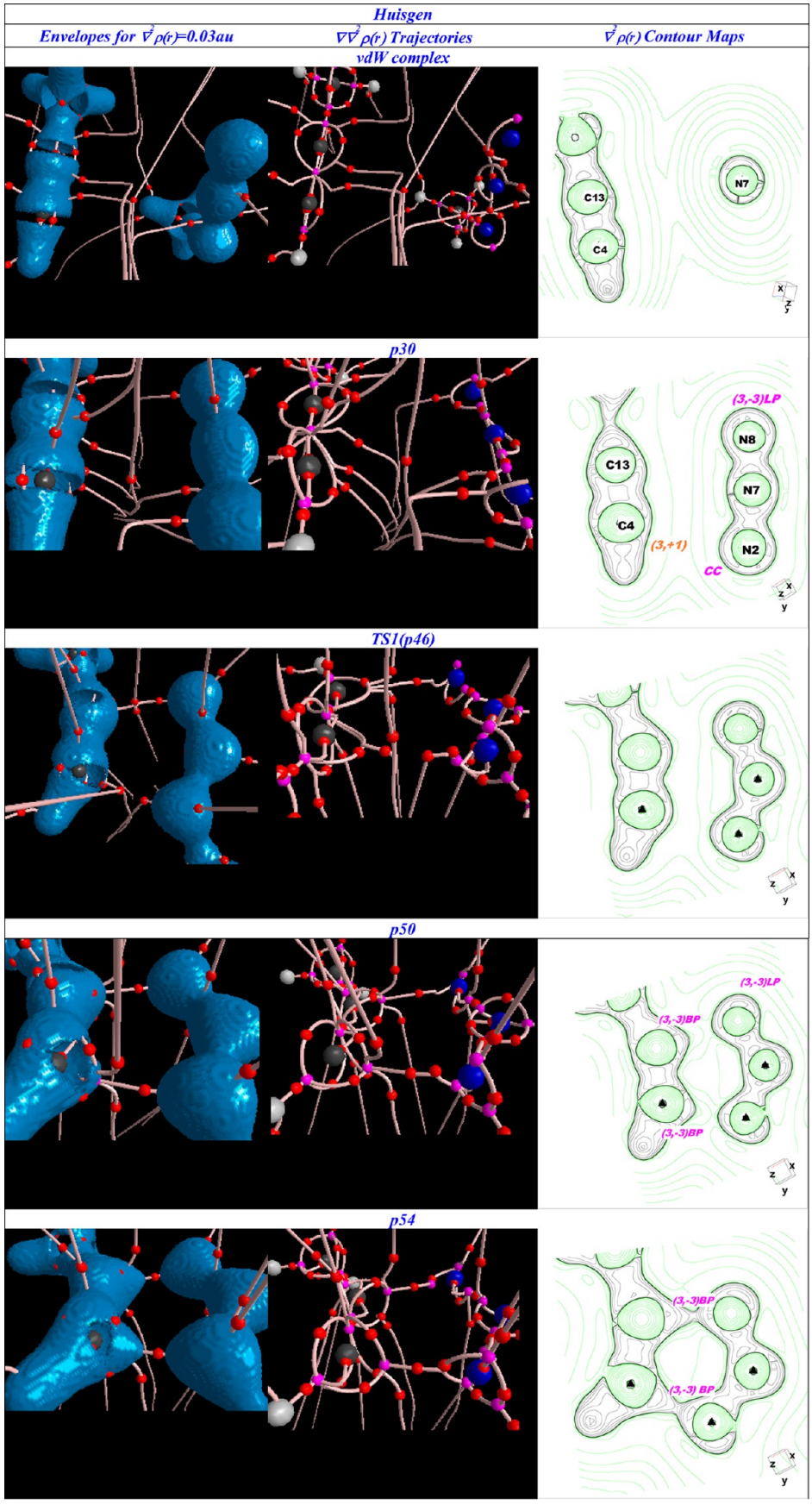


**Figure 3.** continued



DOI: 10.1021/jp5055414
J. Phys. Chem. B 2015, 119, 1243−1258

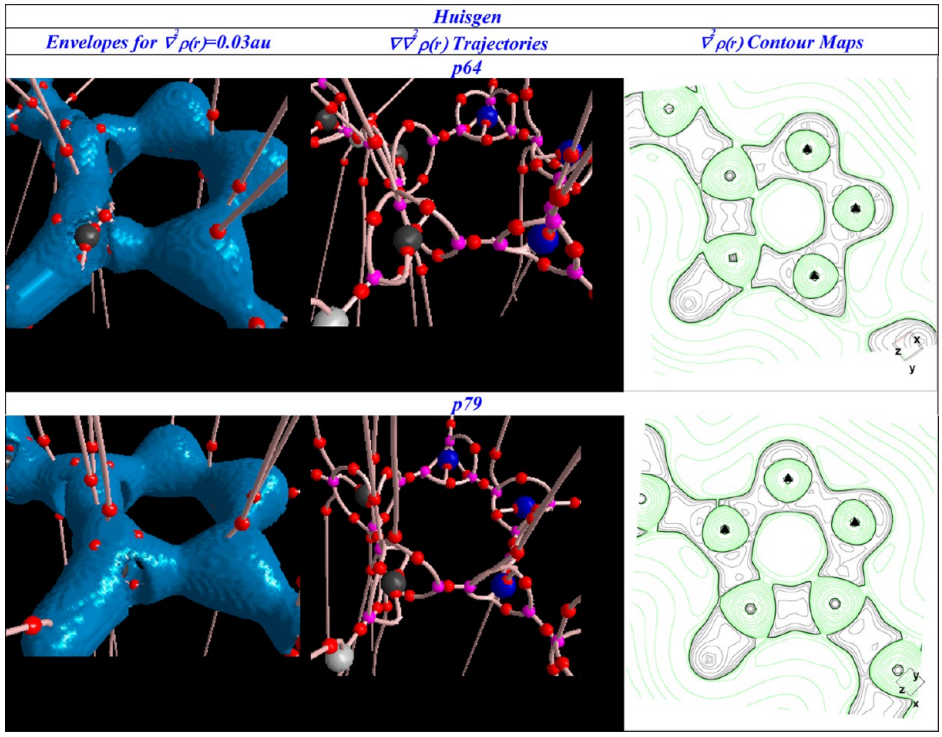


**Figure 3.** Snapshots of envelopes for $\nabla^2\rho(\boldsymbol{r}) = 0.03$, trajectories of $\nabla\nabla^2\rho(\boldsymbol{r})$, and contour maps computed at LC-wPBE(PCM)/6-311++G(3d,p)/6-311++G(d,p) for Huisgen structures chosen along the IRC. For contour maps, green lines denote regions of $\nabla^2\rho(\boldsymbol{r}) > 0$ and black regions of $\nabla^2\rho(\boldsymbol{r}) < 0$. (3, −3) CPs of $L(\boldsymbol{r}) = -\nabla^2\rho(\boldsymbol{r})$ (LP and BP) are plotted in violet, (3, −1) CPs are plotted in red, and (3, +1) and (3, +3) CPs are not shown. Contour maps are computed on N2−C4−C13 and N8−C13−C4 planes.

DFs, respectively (see Figure S1, Supporting Information). Its inability to reproduce cuprophilic interactions has also been recently reported.[18]

**Topological Evolution of $\rho(\boldsymbol{r})$, $\nabla^2\rho(\boldsymbol{r})$, and $\nabla\nabla^2\rho(\boldsymbol{r})$ along the Reaction Coordinate.** The molecular graphs derived from trajectories of the gradient of $\rho(\boldsymbol{r})$, $\nabla\rho(\boldsymbol{r})$ (Figure 2), show that the uncatalyzed process consists of the (practically) simultaneous formation of both covalent bonds, whereas, in the mono- and dinuclear catalyzed counterparts, the catalyst orchestrates first the formation of the external N8−C13, keeping the azide coordinated to it, and the subsequent formation of the internal N2−C4 (see Scheme 1), in a concerted or stepwise fashion depending on the ligands attached to the Cu. The topology of $\rho(\boldsymbol{r})$ does not exhibit a bond critical point (BCP)[25] linking the two Cu atoms. Thereby, from the topology of $\rho(\boldsymbol{r})$, nothing can be said about the bonding between both nuclei.[97−99] Nonetheless, as we will see, some covalency can be inferred from the contour maps of $\nabla^2\rho(\boldsymbol{r})$, and also by computing the delocalization index $\delta(\mathrm{Cu^A}, \mathrm{Cu^B})$. Interestingly, the progressive chemical stability in the molecular formation is accompanied by the topological completion of the molecular graphs (see Figure 2). Conversely, for the 1,4-$Cu_2$AAC from the **Int** to the ***TS4′***, some gradient lines of $\rho(\boldsymbol{r})$ are lost.

**Huisgen Cycloaddition.** This 1,3 dipolar cycloaddition is a concerted reaction, with the formation of the two C−N bonds being practically simultaneous. At the beginning of the process, the reactants are perpendicular to each other (see molecular graphs in Figure 2 and geometries in Figure S2, Supporting Information) and consequently the first stages of the reaction must be devoted to properly orient both fragments in order to align charge concentrations (CCs) or lumps with charge depletions (CDs) or holes, according to the Laplacian complementarity principle.[44] On the contrary, as we will see, the arrangement of the adducts of the catalyzed versions is in good disposition to undergo the reaction (compare the contour maps of $\nabla^2\rho(\boldsymbol{r})$ for ***vdW*** complexes in Figures 3, 4, and 5). Note, in passing, that this complementarity also holds for the ELF,[91] as can be seen in Figure S3 (Supporting Information). Precisely, for the Huisgen at ***p30***, a "double complementarity" is achieved: a gradient line emerges from the N2 atomic graph (and N8 toward C13) toward a hole in C4, that exhibits an sp atomic graph (see Figure 1), and simultaneously, a gradient line from the $\pi$ density of C4−C13 is oriented at the hole in the VSCC of N7. From ***vdW*** to ***p30***, gradient lines from N2 and C4 are approaching each other, whereas the others coming from N8 and C13 are close together from the very beginning. As was indicated in the Quantum Topological Methods section, the converging of two gradient lines would indicate a closed-shell interaction. In fact, the NCI surface (see Figure S4, Supporting Information) and the HOMO and HOMO−1 confirm such a situation (see Figure S5, Supporting Information).

At first sight, the N2−C4 interaction could be seen as a pseudopericyclic contact.[27−29] Nevertheless, several topological and energetic results seem to contradict such a view: (1) although a CC is visualized in the relief maps (see Figure S6, Supporting Information), a proper $(3, -3)_{\mathrm{LP}}$ is not located in the atomic graph of N2 (see also contour map in Figure 3 and relief map in Figure S6, Supporting Information), (2) the hole is not as deep as that typical of pseudopericyclic reactions,[27,28] which (3) from the very beginning appears within the "reactive surface" (given by $\nabla^2\rho(\boldsymbol{r}) = 0$ au surfaces),[44] and (4) the hole is not expanded upon nucleophilic approach.[28,30] In addition, the energetic criterium proposed by Birney[29] of a small or even


DOI: 10.1021/jp5055414
J. Phys. Chem. B 2015, 119, 1243−1258

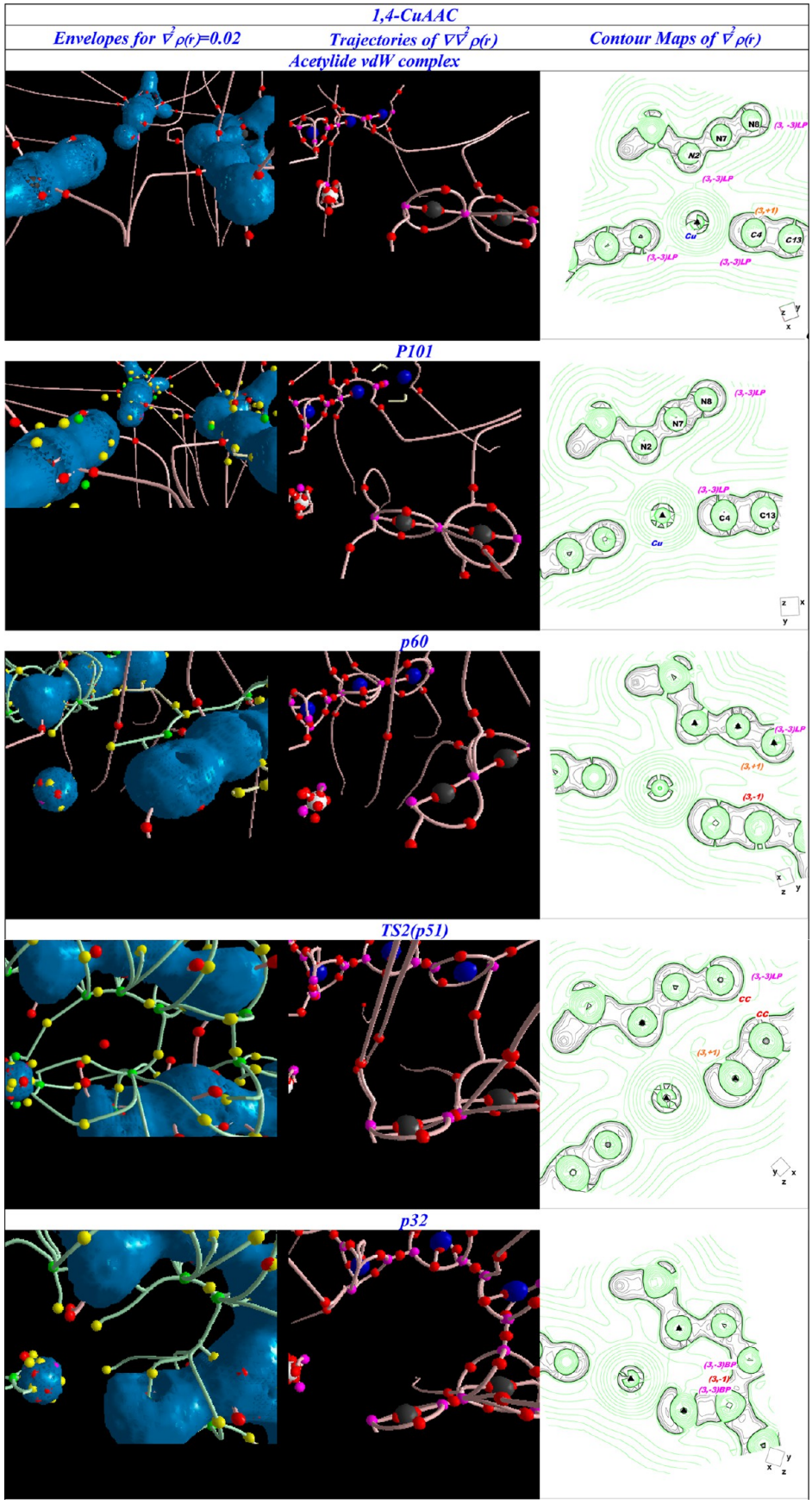


**Figure 4.** continued



DOI: 10.1021/jp5055414
J. Phys. Chem. B 2015, 119, 1243−1258

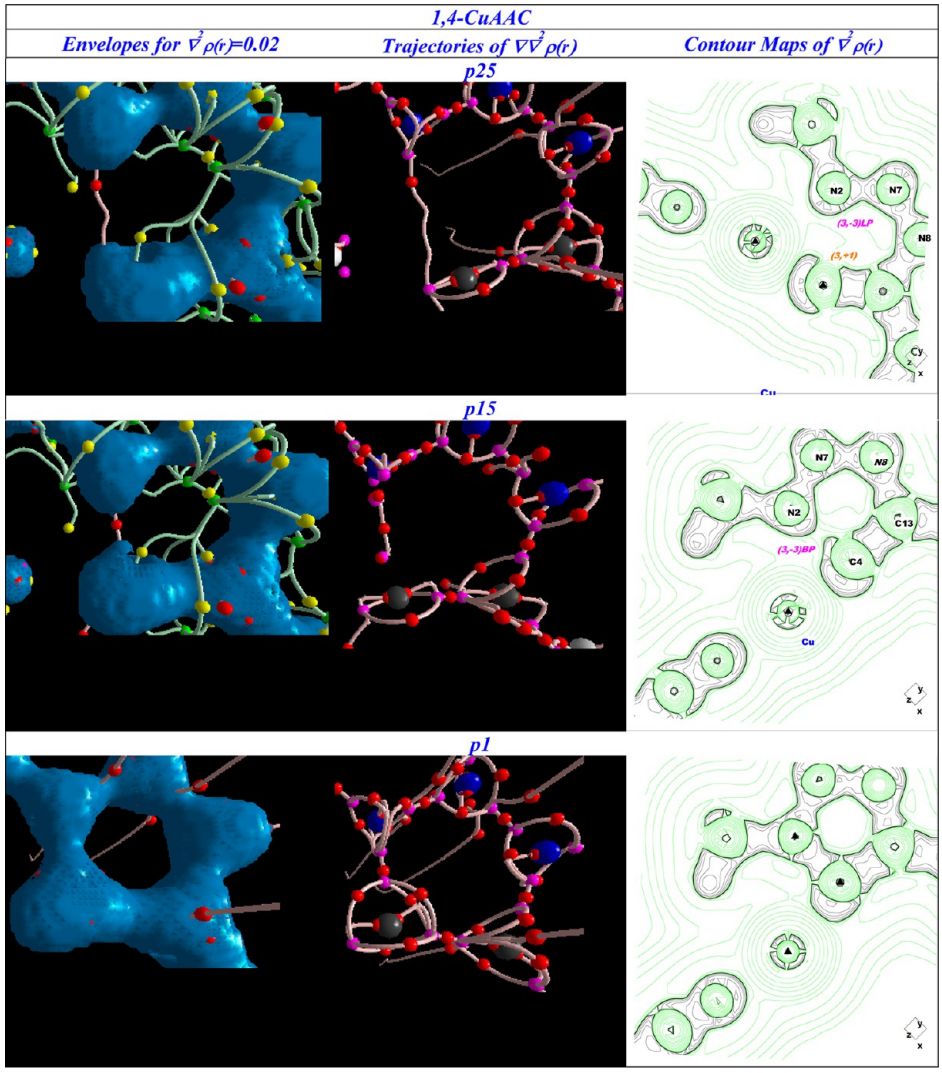


**Figure 4.** Snapshots of contour maps of $\nabla^2\rho(\boldsymbol{r})$ and trajectories of $\nabla\nabla^2\rho(\boldsymbol{r})$ computed at LC-wPBE(PCM)/6-311++G(2d,2p)/6-311++G(d,p) for 1,4-CuAAC for structures chosen along the IRC fot the title reaction with L = $CH_3CN$. For contour maps, green lines denote regions of $\nabla^2\rho(\boldsymbol{r}) > 0$ and black lines denote regions of $\nabla^2\rho(\boldsymbol{r}) < 0$. (3, −3) CPs of $L(\boldsymbol{r}) = -\nabla^2\rho(\boldsymbol{r})$ (LP and BP) are plotted in violet, (3, −1) CPs in red, (3, +1) CPs in yellow, and (3, +3) CPs in green. Contour maps are computed for N2−C4−C13 and N8−C13−C4 planes. For some envelopes, a side view is shown to better appreciate the details.

negligible barrier does not hold. On the other hand, the N8−C13 bond follows a pericyclic-like mode,[27−29] since both atoms posit CCs (see Scheme S1, Supporting Information), as reflected in the gradient trajectories emanating from their atomic graphs. Note that at ***p30*** the topology of $\rho(\boldsymbol{r})$ indicates (see Figure 2) the presence of interactions between the N8 and C13, and C4 and N2 nuclei. However, they would be of the closed-shell type, since gradient trajectories of $\nabla^2\rho(\boldsymbol{r})$ do not overlap, and the values of $\nabla^2\rho(\boldsymbol{r})$ evaluated at the bond critical point are positive and low.[25,97]

At the ***TS1***, the asynchronous formation of both N−C bonds can be appreciated in the trajectories of $\nabla\nabla^2\rho(\boldsymbol{r})$. First, the gradient lines from N8 and C13 collapse starting off the transfer of charge density throughout the interatomic line, also given by trajectories of $\nabla\rho(\boldsymbol{r})$ (see Figure 2). The $\nabla^2\rho(\boldsymbol{r})$ = 0.03 au envelope indicates that charge density has been first accumulated in the atomic graph of C13 to create the new $(3,-3)_{BP}$ to eventually form the bond with N8. On the other side, the gradient trajectories coming from C4 and N2 have not merged yet. The crossing of gradient lines (signaling a singularity[73]) anticipates the creation of the new vertices (see the corresponding $(3,-3)_{BP}$ CPs in ***p50***) in the atomic graphs of C4 and C13. The charge density is subsequently transferred along the interatomic line from ***p50*** to ***p54*** (see contour maps). Furthermore, the gradient lines emerging up and down indicate accumulation in the $\pi$ plane (see MO24 for ***p54*** in Figure S5, Supporting Information). The displacement of charge density from the $(3,-3)_{LP}$ of N8 toward the new face created can be appreciated in the contour map for ***p54***. Topologically, this entails the bifurcation of this nonbonded (3, −3) CP of N8 into a new $(3,-3)_{LP}$ and a bonded (3, −3) CP (compare the contour maps of ***p50*** and ***p54*** in Figure 3) to eventually attain an $sp^2$ atomic graph (see Figure 1).[28] Similar analyses of bifurcations and catastrophes along the reaction coordinate have been reported for $\rho(\boldsymbol{r})$[100] and the ELF[101−103] for several chemical reactions.

Interestingly, the donation of charge of a nucleophile usually depicted by "arrows"[76] encompasses the expansion of its atomic graph[51] with the birth of two new vertices: a $(3,-3)_{LP}$ and another employed to form the new bond given by a $(3,-3)_{BP}$.


DOI: 10.1021/jp5055414
J. Phys. Chem. B 2015, 119, 1243−1258

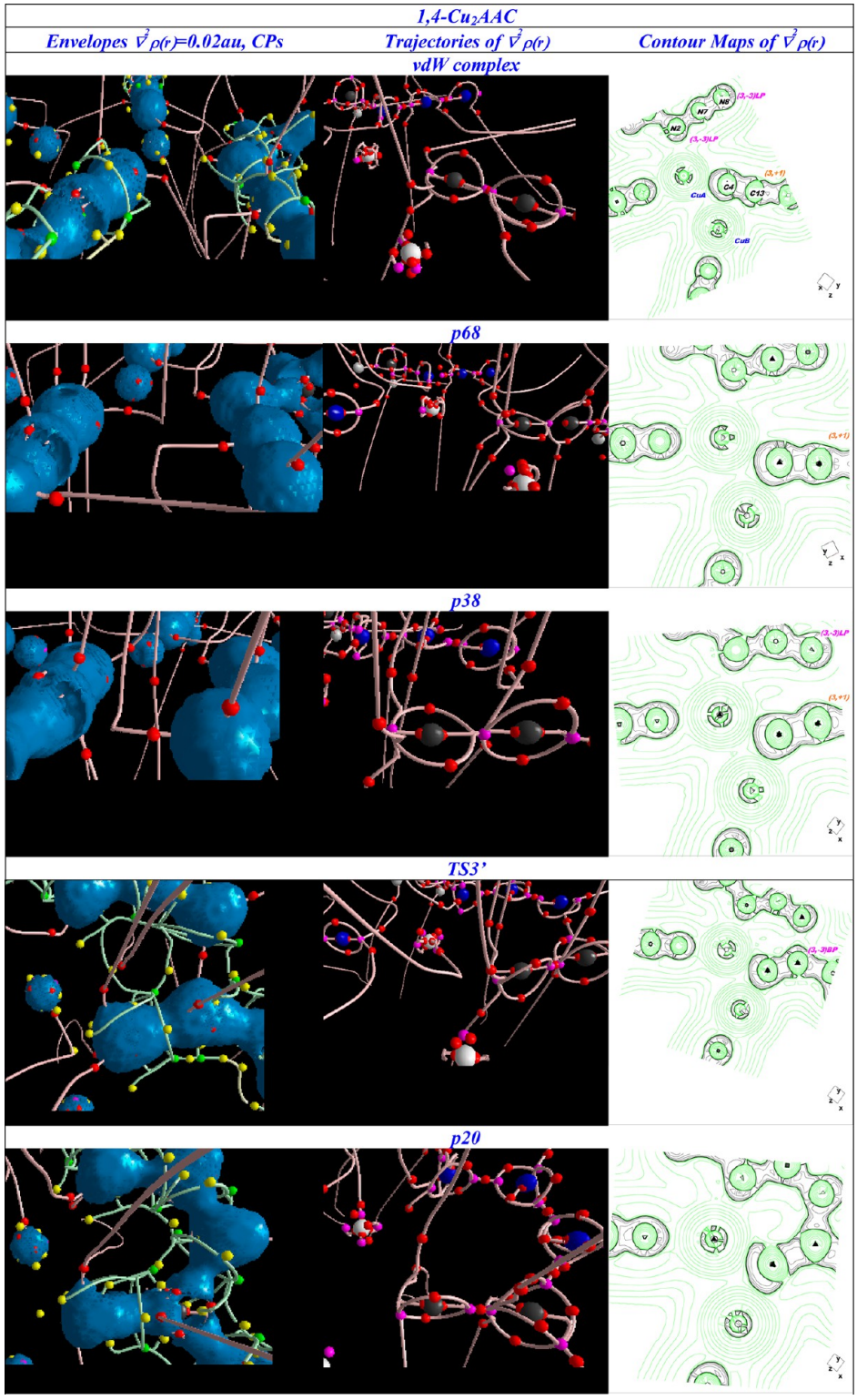


**Figure 5.** continued



DOI: 10.1021/jp5055414
J. Phys. Chem. B 2015, 119, 1243−1258

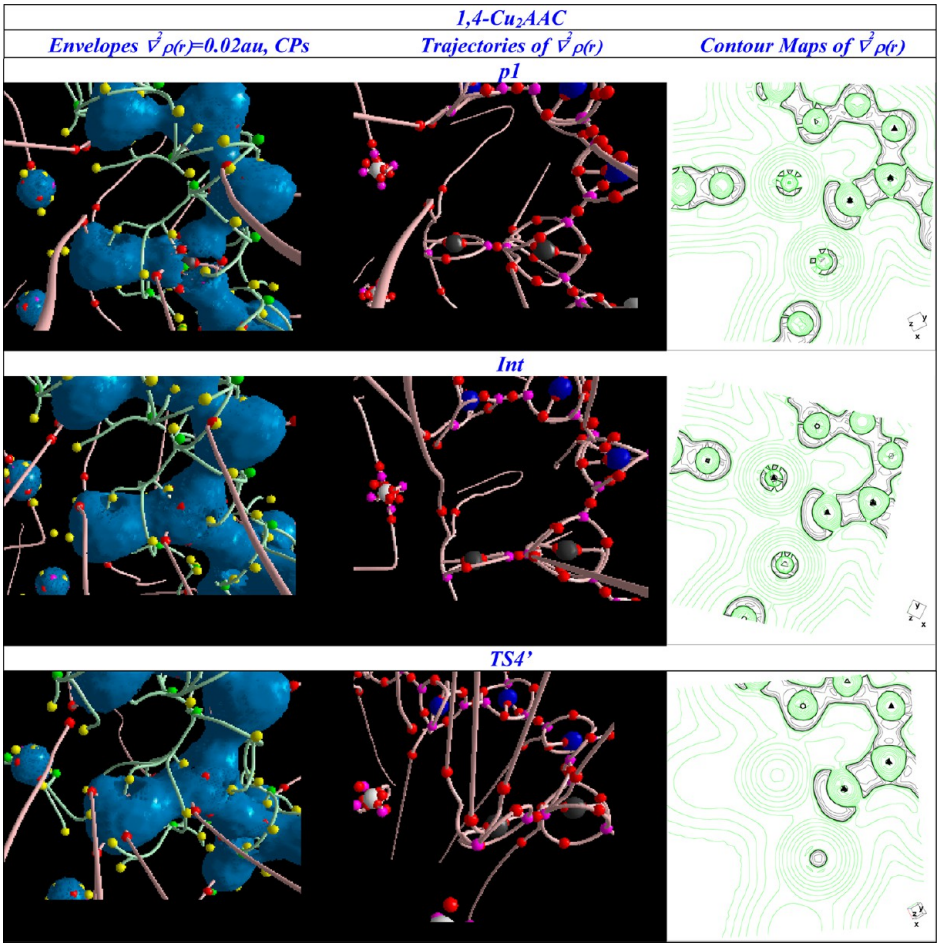


**Figure 5.** Snapshots of envelopes, trajectories of $\nabla\nabla^2\rho(\boldsymbol{r})$ (lateral view), and Contour maps of $\nabla^2\rho(\boldsymbol{r})$ computed at LC-wPBE(PCM)/6-311++G(2d,2p)/6-311++G(d,p) for 1,4-$Cu_2$AAC. For contour maps, green lines denote regions of $\nabla^2\rho(\boldsymbol{r}) > 0$ and black lines denote regions of $\nabla^2\rho(\boldsymbol{r}) < 0$. (3, −3) CPs of $L(\boldsymbol{r}) = -\nabla^2\rho(\boldsymbol{r})$ (LP and BP) are plotted in violet, (3, −1) CPs in red, (3, +1) CPs in yellow, and (3, +3) in green. Contour maps are computed for N8−C13−C4 planes.

At ***p54*** appears the triplet $(3,-3)_{BP}$−(3, −1)−$(3,-3)_{BP}$ of CPs characteristic of a covalent bond,[58,60] indicating that charge density is concentrated along the interatomic line and anticipates the covalent bond formation.[55−59] The rest of the process is aimed at completing the atomic graphs of all the atoms involved, together with the increase of the charge concentration along the interatomic line (see ***p64***). Interestingly, at ***p79***, there is no (3, +1) CP above and below the molecular plane; hence, it could be considered as aromatic. Since the gradient trajectories emerge up and down, the atomic graphs are not of the "pure" benzenic type (see Figure 1). Nonetheless, the gradient trajectories of $\nabla\nabla^2\rho(\boldsymbol{r})$ stand all parallel, indicating the increasing of charge concentration in the same direction. The evolution of some MOs supports this hypothesis (observe the evolution of MO16 from ***TS1*** to ***p79*** in Figure S5, Supporting Information). Therefore, the process would end up providing aromaticity to the product.

**1,4-CuAAC.** A diverse situation is appreciated for the mononuclear catalyzed version of the Huisgen reaction from the very beginning of the process. In the acetylide complex (Figure 4), the Cu(I) coordinates the azide and the ligands (L = $CH_3CN$) through donor−aceptor interactions. In the topology of $\nabla^2\rho(\boldsymbol{r})$, this is reflected in the appearance of $(3,-3)_{LP}$ within the VSCC of the nucleophiles oriented toward a (3, +1) in the VSCD[55,58−60] of the Cu(I). Nonetheless, the degree of coordination of covalency is not the same, as can be seen in the interpenetration of the VSCD (see contour map) of each adduct and in the values of delocalization indices, $\delta(X,Y)$. In fact, the ethylene moiety appears to be better coordinated with Cu through its terminal electronic lone pair ($\delta$(Cu, C4) = 0.899)) than to N2 and N3 ($\delta$(Cu, N2) = 0.318 and $\delta$(Cu, N3) = 0.621). Nonetheless, the mandate for a sigma copper acetylide intermediate also required that a terminal alkyne must be the precursor to generate this complex. As it did occur for the Huisgen, converging gradient lines reveal noncovalent interactions (NCIs)[92] between the fragments (see Figure S4, Supporting Information).

Contrarily to what happened for the Huisgen, from the very beginning, both adducts are in a nice disposition to undergo the process (compare with ***vdW*** for the Huisgen in Figure 3). Further, at the first point selected of both IRCs (i.e., ***p60*** and ***p30***), notable differences arise for the Huisgen and mononuclear 1,4-CuAAC mechanisms. As a consequence of the coordination of N2 to Cu, the internal N is far apart from the ethylene moiety, and thence, the external C−N bond will be created in the first place (this also holds for the 1,4-$Cu_2$AAC, see below), establishing a sequential order in bond formation. Initially, they are bonded by a closed-shell interaction, as seen in the converging gradient trajectories of $\nabla\nabla^2\rho(\boldsymbol{r})$ (see ***p101***) and at ***p60*** through the alignment of CC of C13 toward a hole in N8


DOI: 10.1021/jp5055414
J. Phys. Chem. B 2015, 119, 1243−1258

(see the HOMO in Figure S7, Supporting Information) Furthermore, the formation of N8−C13 appears now to follow a pseudopericyclic mechanism but, remarkably, with the C13 acting as the nucleophile. In fact, for the 1,4-CuAAC, two gradient lines emerging from the atomic graph of C13 (from a (3, −1) CP) are directed at a (3, +1) CP within the VSCC of N8 (sp type, Figure 1), pointing out the nucleophilic activity of C13 as suggested by Worrell et al.[21] Furthermore, the envelope for $\nabla^2\rho(\boldsymbol{r})$ = 0.02 au shows that the hole is nonexistent, since no (3, +1) CP is located in the VSCC of the carbon atom. On the contrary, for the Huisgen, two gradient lines emanated from N8 and C13 (see ***p30*** in Figure 3), being more close to a pericyclic contact (see Scheme S1, Supporting Information). As a consequence, to form the N8−C13 bond in the 1,4-CuAAC, charge density must be displaced from the contiguous double C4−C13 (see contour map for ***p51*** (TS2) in Figure 4, and compare with the ***p32***, and ***p25***), provoking the creation of a hole in the VSCC of C4, that would entail the modification of the original Huisgen mechanism.

Though concerted, the enhanced asynchronicity of bond formation for the 1,4-CuAAC is appreciated in the TS. In addition, in the TS, C13 and N8 appear to be linked by a gradient trajectory, thus starting off the formation of the covalent bond, by transferring charge density throughout the interatomic line that binds both nuclei (see Figure 2).

From the TS downward, the catalytic activity of copper turns, more clearly, the mechanism of the internal bond formation into a pseudopericyclic mode (see Scheme S1, Supporting Information).[27−29] Interestingly, while keeping the azide coordinated, the Cu drives the nucleophilic N2 toward the hole at C4 (which could be conceived as a Fischer carbene[61]) in an energy-free motion, that corresponds to the "shoulder" in the energy profile (see Chart 1, entry A). In fact, from ***p32*** to ***p25***, the degree of coordination as measured by the delocalization index between the azide and the Cu(I) diminishes (compare contour maps in Figure 4), passing the $\delta$(Cu−N2) from 0.529 to 0.409. Conversely, $\delta$(N2, C4) goes from 0.291 to 0.439 and $\delta$(C4, Cu) from 1.103 to 1.022 at ***p32*** and ***p25***, respectively. Interestingly, the hole is enlarged by the approach of the nucleophile (compare ***p51(TS2)***, ***p32***, and ***p25***). This could be envisaged as a "dynamic" version of the Pearson's HSAB principle[104] and seems to be ubiquitous in pseudopericyclic reactions:[27−29] as long as the nucleophile (base) goes softer, the electrophile (acid) becomes softer. This is reflected in the evolution of the first eigenvalue of the Hessian of $\nabla^2\rho(\boldsymbol{r})$.[36] For the $(3,-3)_{LP}$, the $\lambda_1$ decreases along the reaction coordinate: $\lambda_1$(***p101***) = −33.899 au, $\lambda_1$(***p48***) = −30.26 au, $\lambda_1$(***p32***) = −29.04 au, $\lambda_1$(***p25***) = −28.17 au, $\lambda_1$(***p15***) = −24.37 au, whereas for the (3, +1) it increases approaching to zero, thus becoming a "true hole": $\lambda_1$(***p101***) = −19.42 au, $\lambda_1$(***p60***) = −19.37 au, $\lambda_1$(***p48***) = −1.79 au, $\lambda_1$(***p32***) = −0.86 au (see the relief maps in Figure S8, Supporting Information). This effect is especially observed after the TS up to ***p15***. Finally, the $(3,-3)_{LP}$ of N2 and C4 undergo a bifurcation to yield new $(3,-3)_{BP}$ and $(3,-3)_{LP}$ CPs (see ***p15***).[28] Note also that here the C4 also plays the role of a typical nucleophile in other pseudopericyclic reactions, suffering a splitting of one of its (3, −3) CPs to expand its atomic graph. In fact, at ***p25***, the $\lambda$(C4) has been substantially increased to 4.523, probably to employ charge density in the bond formation.

In sum, the copper modifies the original Huisgen mechanism by inducing a sequential order in the N−C bond formation through pseudopericyclic mechanisms clearly asynchronic but, notwithstanding, concerted when the ligand attached to copper is acetonitrile. The novelty is that the former pseudopericyclic mechanism encompasses a carbon atom as a donor of charge density.

**1,4-$Cu_2$AAC.** The reaction paths computed at the LCwPBE/6-311++G(d,p) theoretical level showed that upon inclusion of a second Cu atom the original concerted mechanism for the 1,4-CuAAC (with $CH_3CN$) is turned into a stepwise mechanism (see Chart 1). It should be remembered that the 1,4-$Cu_2$AAC (with $CH_3CN$) is the only process predicted to follow a stepwise mechanism at our best level of theory (i.e., LC-wPBE(PCM)/6-311G++(d,p)), albeit with an activation enthalpy difference of only 0.39 kcal/mol with respect to the concerted 1,4-CuAAC.

First, in view of the topology of $\nabla^2\rho(\boldsymbol{r})$ and $\nabla\nabla^2\rho(\boldsymbol{r})$, the second Cu atom ($Cu^B$) does not appear to be attached to the $\pi$ density (see Figure 5 and also the relief maps in Figure S9, Supporting Information) of C4−C13 as suggested by Fokin et al.[3] but is coordinated to the LP of the C4. Nonetheless, the intrinsic complexity of the metal bond between $Cu^B$ and the ethylene moeity can be appreciated in HOMO, MO74, and MO71 for vdW in Figure S10 (Supporting Information). Crucially, as can be seen in the contour map for the vdW complex (see Figure 5), some amount of the charge concentrated in the LP of C4 is polarized toward the second Cu atom, $Cu^B$. Thus, the coordination of the second Cu causes the spreading of the LP of C4, that is also reflected in the increase of the number of gradient lines of $\nabla^2\rho(\boldsymbol{r})$ departing from the $(3,-3)_{LP}$ of C4. A quantitative measure can be given by the first eigenvalue of the Hessian matrix of $\nabla^2\rho(\boldsymbol{r})$,[36] associated with the perpendicular direction of the eigenvector to the molecular plane. For the vdW complexes, $\lambda_1$ amounts to −8.05 au and −7.75 au for the 1,4-CuAAC and 1,4-$Cu_2$AAC, respectively. Hence, the $(3,-3)_{LP}$ exhibits a larger spreading for the 1,4-$Cu_2$AAC, becoming a softer base,[36] and the hole is reduced, becoming a harder acid. The delocalization indices provide further support: the binding of the $Cu^A$ by the carbene-like C4 is now affected by the second Cu atom: $\delta(Cu^A, C4)$ = 0.79 for 1,4-$Cu_2$AAC vs 0.899 for 1,4-CuAAC. The covalency between both coppers ($\delta(Cu^A, Cu^B)$ = 0.19) is lower than the reported values for typical ionic bonds such as in NaF.[105] The value of $\delta(Cu^A, C13)$ = 0.1 for the delocalization index between $Cu^A$ and C13 could indicate the involvement of the double C4−C13 bond. The debilitated binding of the C4 with $Cu^A$ forces a stronger coordination by the N2 through its $(3,-3)_{LP}$: in fact, $\delta(Cu^A, N2)$ amounts now to 0.399 vs 0.318 for 1,4-CuAAC. This would be of importance in the stability of the intermediate (***Int***) afterward.

As a consequence, upon inclusion of the second copper, the mechanism of formation of both N−C bonds for the 1,4-CuAAC will be altered. As a matter of fact, the formation of the external N−C will follow a pseudopericyclic mechanism but now with the roles of eletrophile and nucleophile inverted. In particular, from the very beginning, the C13 exhibits an sp-type atomic graph (see Figure 1) with a hole facing off the N8 (see Figure 5), thus playing the role of the electrophile. In fact, the envelope $\nabla^2\rho(\boldsymbol{r})$ = 0.02 au indicates that now the C13 exhibits a hole in its VSCC for the ***vdW*** (compare with ***vdW*** in Figure 4) that is even enlarged for ***p68*** (compare the atomic graphs in Figure 5). In fact, the charge density localized within its basin diminishes for the first point of the IRC ($\lambda$(C13) = 4.26 for ***p101*** vs 4.10 for ***p68***).[21] This can be rationalized by the amount of charge density needed to coordinate the two Cu atoms. Precisely, the charge density localized in the basin of the C4,


DOI: 10.1021/jp5055414
J. Phys. Chem. B 2015, 119, 1243−1258

$\lambda$(C4), amounts to 4.19 at ***p68*** for 1,4-$Cu_2$AAC vs 4.30 for 1,4-CuAAC at ***p101***. Besides, the covalency[60] between both centers as measured by the delocalization indices $\delta$(C4, C13) amounts to 2.38 for the 1,4-CuAAC vs 2.17 for the 1,4-$Cu_2$AAC. All of these reults seem to point to a displacement of charge density toward C4 aimed at coordinating the $Cu^B$. Consequently, the formation of the terminal N−C entails the inversion of nucleophilic and electrophilic roles of the C13 and N8 as compared with that encountered in the mononuclear 1,4-CuAAC.

At the second point chosen in the IRC, ***p38***, the N8 is more involved in the bond formation, and a gradient line departing from the $(3,-3)_{LP}$ of its atomic graph goes toward the VSCD of the C13, which exhibits an sp atomic graph with a hole, given by a $(3,+1)$ CP, in the middle of the face (see Figure 5). The molecular graph, as given by trajectories of $\nabla\rho(\boldsymbol{r})$, exhibits an interatomic line joining both centers (see Figure 1) and in the HOMO, the $\pi$ density of C4−C13 overlaps with the atomic p orbital of N8 within the molecular plane (see Figure S10, Supporting Information). However, as can be appreciated in the atomic graph of N8, some bending of the gradient line indicates accumulation of charge—coming from the $(3,-3)_{LP}$—in that face.

At the ***TS3′***, the atomic graphs of N and C appear to be united by a gradient trajectory, iniating thus the transfer of charge density along the interatomic line to eventually create a covalent bond (see the contour map). The topology of $\nabla\nabla^2\rho(\boldsymbol{r})$ shows that the formation of the internal N−C bond is more advanced for the 1,4-$Cu_2$AAC process: three degenerate (i.e., non-Morse[71]) $(3,-1)-(3,-3)-(3,-1)$ CPs in the $\nabla^2\rho(\boldsymbol{r})$ appear within the face of the C13, and some bending can be appreciated in the gradient trajectory emerging from the $(3,-3)_{LP}$ of N8, indicating charge accumulation within the face of the polyhedron. This is visualized in the tiny lump of CC in the relief map of $L(\boldsymbol{r}) = -\nabla^2\rho(\boldsymbol{r})$ (see Figure S9, Supporting Information). In fact, the delocalization index $\delta$(C13, N8) amounts to 0.544 and 0.463 for the 1,4-$Cu_2$AAC and 1,4-CuAAC, respectively, indicating a larger covalency between C13 and N8.

At ***p20***, the external N−C bond appears to be formed, with the corresponding triplet $(3,-3)_{BP}-(3,-1)-(3,-3)_{BP}$ that characterizes a covalent bond.[28,58,60] On the other hand, some polarization of the charge density of the lone pair of C4 seems to be displaced toward the $Cu^B$ atom (see contour map). Notice that the $(3,-3)_{LP}$ of N2 is not so good oriented toward the hole. As it was pointed out for the vdW complex, the $Cu^A$ necessitates more stabilization from N2 and, hence, the covalency with N2, $\delta(Cu^A, N2)$ increases dramatically from 0.399 for ***vdW*** to 0.667 for ***p20***.

The process stops at ***Int*** (see Scheme 1). We conjecture that the minor size of the hole (compare with ***p25*** in Figure 4) and the bad orientation of the $(3,-3)_{LP}$ of N2 toward it, as seen by the orientation of the gradient trajectories of $\nabla\nabla^2\rho(\boldsymbol{r})$, can be the cause of this behavior.

## SUMMARY AND CONCLUSIONS

Summing up, the catalyzed mononuclear and dinuclear versions of the Huisgen reaction (the 1,4-CuAAC and 1,4-$Cu_2$AAC) have been thoroughly investigated with quantum topological methods with several density functionals (B3LYP, M06-2X, M06-L, LCwPBE, wB97XD). Unfortunately, the B3LYP DF is not suitable for these types of processes, for it does not discern between stepwise and concerted depending on the reaction conditions and does not reproduce vdW interactions. In view of the small difference in the activation enthalpies (0.39 kcal/mol) computed at the LCwPBE/6-311++G(d,p) theory level, we contend that the concurrence of monuclear and dinuclear processes is feasible.

It has been shown that the own catalytic activity of Cu in 1,4-CuAAC and $Cu^A$ and $Cu^B$ in 1,4-$Cu_2$AAC can be traced back by following the evolution of the topology of $\nabla^2\rho(\boldsymbol{r})$ and $\nabla\nabla^2\rho(\boldsymbol{r})$ along the reaction coordinate.

First, for the 1,4-CuAAC, the copper, while keeping the azide coordinated to it, orchestrates first the formation of the external N−C bond, where carbon acts as a nucleophile toward N by a novel pseudopericyclic mode of reaction. The displacement of charge needed to form the internal bond provokes a hole in the terminal carbon of the alkyne that leads the internal N of the azide to attack the hole by a pseudopericyclic mechanism in a concerted asynchronous process that could be turned into a stepwise process depending on the nature of the ligands and the solvent. Second, for the 1,4-$Cu_2$AAC, to properly coordinate both coppers, the carbene-like terminal C of ethylene must spread out its lone pair. This causes the hole at the C to be narrower, and forces the internal N of the azide to be more strongly coordinated to $Cu^A$. As a consequence, the concerted motion of the internal N toward the hole at the electrophilic carbon atom does not happen and an intermediate appears to be in the reaction coordinate, turning the process into stepwise. Once the intermediate is formed, the activation enthalpy toward the triazole is practically negligible. Therefore, the stability of the intermediate appears to be crucial in determining which mechanism is predominant.

The very important conclusion is that this intriguing reaction shows a chameleonic mechanism depending on the conditions and that the catalyst transforms the pericyclic contacts of the Huisgen mechanism into pseudopericyclic contacts.

## ASSOCIATED CONTENT

### Supporting Information

A classification of pseudopericyclic reaction types; electronic energies and enthalpies computed for all the points along the IRC with the B3LYP, wB97XD, M06-2X, and B3LYP for the 1,4-CuAAC and with LCwPBE for the 1,4-CuAAC and 1,4-$Cu_2$AAC; geometries computed with the DFs utilized (B3LYP, M06-2X, and LCwPBE); geometries correponding to the molecular graphs selected; ELF envelopes for several points of the Huisgen; NCI surfaces for the vdW complex of the Huisgen, 1,4-CuAAC, and 1,4-$Cu_2$AAC; relief maps for selected points of the three processes; natural MOs; and Cartesian coordinates for all reported structures. This material is available free of charge via the Internet at http://pubs.acs.org.

## AUTHOR INFORMATION

### Corresponding Author

*Phone: +34952131866. Fax: +34952132000. E-mail: quirante@uma.es.

### Notes

The authors declare no competing financial interest.

## ACKNOWLEDGMENTS

The authors are thankful for generous allocation time in Picasso Supercomputer at Malaga's University and also thank Administrator Rafael Larrosa for his prompt and efficient



DOI: 10.1021/jp5055414
J. Phys. Chem. B 2015, 119, 1243−1258

response. S.C.-L. also wants to thank Manuela Jiménez Garcés for her patience.

## REFERENCES


(1) Hein, J. E.; Fokin, V. V. Copper-catalyzed Azide−Alkyne Cycloaddition (CuAAC) and Beyond: New Reactivity of Copper(I) Acetylides. *Chem. Soc. Rev.* **2010**, *39*, 1302−1315.

(2) Tornøe, C. W.; Christensen, C.; Meldal, M. Peptidotriazoles on Solid Phase: [1,2,3]-Triazoles by Regiospecific Copper(I)-Catalyzed 1,3-Dipolar Cycloadditions of Terminal Alkynes to Azides. *J. Org. Chem.* **2002**, *67*, 3057.

(3) Rostovtsev, V. V.; Green, L. G.; Fokin, V. V.; Sharpless, K. B. A Stepwise Huisgen Cycloaddition Process:Copper(I)-Catalyzed Regioselective "Ligation" of Azides and Terminal Alkynes. *Angew. Chem., Int. Ed.* **2002**, *41*, 2596−2599.

(4) Meldal, M.; Tornøe, C. W. Cu-Catalyzed Azide-Alkyne Cycloaddition. *Chem. Rev.* **2008**, *108*, 2952−3015.

(5) Himo, F.; Lovell, T.; Hilgraf, R.; Rostovtsev, V. V.; Noodleman, L.; Sharpless, K. B.; Fokin, V. V. Copper(I)-Catalyzed Synthesis of Azoles. DFT Study Predicts Unprecedented Reactivity and Intermediates. *J. Am. Chem. Soc.* **2005**, *127*, 210−216.

(6) Hein, J. E.; Tripp, J. C.; Krasnova, L. B.; Sharpless, K. B.; Fokin, V. V. Copper(I)-Catalyzed Cycloaddition of Organic Azides and 1-Iodoalkynes. *Angew. Chem., Int. Ed.* **2009**, *48*, 8018−8021.

(7) Spiteri, C.; Moses, J. E. Copper-Catalyzed Azide-Alkyne Cycloaddition: Regioselective Synthesis of 1,4,5-Trisubstituted 1,2,3-Triazoles. *Angew. Chem., Int. Ed.* **2010**, *49*, 31−33.

(8) Kuang, G.-C.; Guha, P. M.; Brotherton, W. S.; Simmons, J. T.; Stankee, L. A.; Nguyen, B. T.; Clark, R. J.; Zhu, L. *J. Am. Chem. Soc.* **2011**, *133*, 13984−14001.

(9) Rodionov, V. O.; Fokin, V. V.; Finn, M. G. Mechanism of the Ligand-Free $Cu^{I}$-Catalyzed Azide-Alkyne Cycloaddition Reaction. *Angew. Chem., Int. Ed.* **2005**, *44*, 2211−2215.

(10) Díez-González, S. Well-Defined Copper(I) Complexes for Click Azide-Alkyne Cycloaddition Reactions: One Click Beyond. *Catal. Sci. Technol.* **2011**, *1*, 166−178.

(11) Liang, L.; Astruc, D. The Copper(I)-Catalyzed Alkyne-Azide Cycloaddition (CuAAC) "Click" Reaction and Its Applications. An Overview. *Coord. Chem. Rev.* **2011**, *255*, 2933−2945.

(12) Ji, P.; Atherton, J. H.; Page, M. I. Copper Catalysed Azide−Alkyne Cycloaddition (CuAAC) in liquid ammonia. *Org. Biomol. Chem.* **2012**, *10*, 7965−7969.

(13) Chiappe, C.; Mennucci, B.; Pomelli, C. S.; Sanzonea, A.; Marra, A. A Theoretical Study of the Copper(I)-catalyzed 1,3-Dipolar Cycloaddition Reaction in Dabco-Based Ionic Liquids: the Anion Effect on Regioselectivity. *Phys. Chem. Chem. Phys.* **2010**, *12*, 1958−1962.

(14) Becke, B. V. D. Density-functional Exchange-Energy Approximation with Correct Asymptotic Behavior. *Phys. Rev. B* **1988**, *38*, 3098−3099.

(15) Becke, B. V. D. Density Functional Thermochemistry. III. The Role of Exact Exchange. *J. Chem. Phys.* **1993**, *98*, 5648−5652.

(16) Lee, C.; Yang, W.; Parr, R. G. Development of the Colle-Salvetti Correlation-Energy Formula into a Functional of the Electron Density. *Phys. Rev. B* **1988**, *37*, 785−789.

(17) Parr, R. G.; Yang, W. *Density-Functional Theory of Atoms and Molecules*; Oxford University Press: New York, 1989.

(18) Straub, B. F. $\mu$-Acetylide and $\mu$-Akenylidene Ligands in 'Click' Triazole Syntheses. *Chem. Commun.* **2007**, 3868−3870.

(19) Cantillo, D.; Ávalos, M.; Babiano, R.; Cintas, P.; Jiménez, J. L.; Palacios, J. C. Assessing the Whole Range of CuAAC Mechanisms by DFT Calculations—On the Intermediacy of Copper Acetylides. *Org. Biomol. Chem.* **2011**, *9*, 2952−2958.

(20) Özen, C.; Tüzün, N. S. The Mechanism of Copper-Catalyzed Azide-Alkyne Cycloaddition Reaction: A Quantum Mechanical Investigation. *J. Mol. Graphics Modell.* **2012**, *34*, 101−107.

(21) Worrell, B. T.; Malik, J. A.; Fokin, V. V. Direct Evidence of a Dinuclear Copper Intermediate in Cu(I)-Catalyzed Azide-Alkyne Cycloadditions. *Science* **2013**, *340*, 457−460.

(22) Dedola, S.; Nepogodievand, S. A.; Field, R. A. Recent Applications of the CuI-Catalysed Huisgen Azide−Alkyne 1,3-Dipolar Cycloaddition Reaction In Carbohydrate Chemistry. *Org. Biomol. Chem.* **2007**, *5*, 1006−1017.

(23) Santoyo-González, F.; Hernandez-Mateo, F. Azide−Alkyne 1,3-Dipolar Cycloadditions: a Valuable Tool in Carbohydrate Chemistry. *Top. Heterocycl. Chem.* **2007**, *7*, 133−177.

(24) Pino-González, M. S.; Assiego, C.; Oña, N. Studies on Reactivity of Azidoamides, Intermediates In the Synthesis of Tetrahydroxypipecolic Acid Derivatives. *Tetrahedron: Asymmetry* **2008**, *19*, 932−937.

(25) Bader, R. F. W. *Atoms in Molecules: a Quantum Theory*; Oxford University Press: Oxford, U.K., 1990.

(26) Lemal, D. An Extraordinarily Facile Sulfoxide Automerization. *J. Am. Chem. Soc.* **1976**, *98*, 4325−4327.

(27) Calvo-Losada, S.; Quirante, J. J. Pericyclic versus Pseudopericyclic Reactions. What the Laplacian of the Charge Density, $\nabla^2\rho(\mathbf{r})$, Has To Say about It? The Case of Cycloaddition Reactions. *J. Phys. Chem. A* **2008**, *112*, 8164−8178.

(28) Calvo-Losada, S. Reacciones Pericíclicas vs. Pseudopericíclicas: Estudio Químico Cuántico Topológico. Ph.D. Thesis, University of Málaga, Málaga, Spain, 2011.

(29) Birney, D. M.; Wagenseller, P. E. Pericyclic and Pseudopericyclic Thermal Cheletropic Decarbonylations: When Can a Pericyclic Reaction Have a Planar, Pseudopericyclic Transition State? *J. Am. Chem. Soc.* **1997**, *119*, 4509−4517.

(30) Calvo-Losada, S.; Pino-González, M. S.; Quirante, J. J. On the regioselectivity of the Mononuclear Copper-Catalyzed Cycloaddition of Azide and Alkynes (CuAAC). A Quantum Chemical Topological Study. *J. Mol. Model.* **2014**, *20*, 2187.

(31) Jencks, W. P. When Is an Intermediate Not an Intermediate? Enforced Mechanisms of General Acid-Base Catalyzed, Carbocation, Carbanion, and Ligand Exchange Reactions. *Acc. Chem. Res.* **1980**, *13*, 161−169.

(32) Jencks, W. P. How Does a Reaction Choose Its Mechanism? *Chem. Soc. Rev.* **1981**, *10*, 345−375.

(33) Young, P. R.; Huang, H. C. Iodide Reduction of Sulfilimines. 2. Evidence for Concurrent Stepwise and Concerted Mechanisms for the Decomposition of Sulfurane Intermediates. *J. Am. Chem. Soc.* **1987**, *109*, 1805−1809.

(34) Bader, R. F. W. Quantum Topology of Molecular Charge Distributions. III. The mechanics of an atom in a Molecule. *J. Chem. Phys.* **1980**, *73*, 2871−2883.

(35) Srebrenik, S.; Bader, R. F. W.; Nguyen-Dang, T. T. Subspace Quantum Mechanics and the Variational Principle. *J. Chem. Phys.* **1978**, *68*, 3667.

(36) Bader, R. F. W.; MacDougall, P. J.; Lau, C. D. H. Bonded and Nonbonded Charge Concentrations and Their Relation to Molecular Geometry and Reactivity. *J. Am. Chem. Soc.* **1984**, *106*, 1594−1605.

(37) Popelier, P. L. A. On the Full topology of the Laplacian of the Electron Density. *Coord. Chem. Rev.* **2000**, *197*, 169−189.

(38) Malcolm, N. O. J.; Popelier, P. L. A. On the Full topology of the Laplacian of the electron density II: Umbrella Inversion of the Ammonia Molecule. *J. Phys. Chem. A* **2001**, *105*, 7638−7645.

(39) Bader, R. F. W. Professor Gillespie-A Symbiotic Relationship. *Coord. Chem. Rev.* **2000**, *197*, 71−94.

(40) Shi, Z.; Boyd, R. J. The Shell Structure of Atoms and the Laplacian of the Charge Density. *J. Chem. Phys.* **1987**, *88*, 4375.

(41) Sagar, R. P.; Ku, A. C. T.; Smith, V. H., Jr.; Simas, A. M. The Laplacian of the Charge Density and Its Relationship to the Shell Structure of Atoms and Ions. *J. Chem. Phys.* **1988**, *88*, 4367.

(42) Eickerling, G.; Reiher, M. The Shell Structure of Atoms. *J. Chem. Theory Comput.* **2008**, *4*, 286−296.

(43) Popelier, P. L. A.; Burke, J.; Malcom, N. O. J. Functional Groups Expressed as Graphs Extracted from the Laplacian of the Electron density. *Int. J. Quantum Chem.* **2003**, *92*, 326−336.

(44) Bader, R. F. W.; Popelier, P. L. A.; Chang, C. Similarity and Complementarity in Chemistry. *J. Mol. Struct.: THEOCHEM* **1992**, *87*, 145−171.




DOI: 10.1021/jp5055414
*J. Phys. Chem. B* 2015, 119, 1243−1258

(45) Gatti, C.; Barzaghi, M.; Bonati L.; Pitea, D. On the Chemical Nature of Transition States in Cycloaddition Reactions: A Charge Density Topological Approach. Application to the Thermal Cycloaddition of two Ethylenes and to the Diels-Alder Reaction of Butadiene and Ethylene. In Quantum Chemistry: Basis Aspects, Actual Trends: Proceedings of an International Workshop on Quantum Chemistry, Girona, Spain; Carbó, R., Ed.; *Stud. Phys. Theor. Chem.* **1989**, *62*, 401.
(46) Carroll, M. T.; Cheeseman, J. R.; Osman, R.; Weistein, H. Nucleophilic Addition to Activated Double Bonds: Predictions of Reactivity from the Laplacian of the Charge Density. *J. Phys. Chem.* **1989**, *93*, 5120−5123.
(47) Shi, Z.; Boyd, R. J. The Laplacian of the Charge Density as a Probe of Reaction Paths and Reactivity: A comparison of $SN_2$ Reactions at C and Si. *J. Phys. Chem.* **1991**, *95*, 4698−4701.
(48) Aray, Y.; Murchich, J. Nucleophilic Attack on the Cyano Group. A Description in Terms of the Laplacian of the Molecular Charge Density. *J. Mol. Struct.: THEOCHEM* **1993**, *27*, 229−233.
(49) Tanga, T.-H.; Fu, X. Theoretical Studies on Nucleophilic Vinylic Fluoride Substitution. *J. Mol. Struct.: THEOCHEM* **1997**, *392*, 152−167.
(50) Calvo-Losada, S.; Quirante, J. J. DFT Study of Competive Wolff Rearrangement and [1,2]-Hydrogen Shift of $\beta$-oxy-$\alpha$-Diazo Carbonyl Compounds. *J. Mol. Struct.: THEOCHEM* **1997**, *398*−*399*, 435−443.
(51) Cortés-Guzmán, F.; Gómez, R. M.; Rocha-Rinza, T.; Sánchez-Obregón, M. A.; Guevara-Vela, J. M. Valence Shell Charge Concentration (VSCC) Evolution: A Tool to Investigate the Transformations within a VSCC Throughout a Chemical Reaction. *J. Phys. Chem. A* **2011**, *115*, 12924−12932.
(52) Gillespie, R. J.; Bytheway, I.; DeWitte, R. S.; Bader, R. F. W. Trigonal Bipyramidal and Related Molecules of the Main Group Elements: Investigation of Apparent Exceptions to the VSEPR Model through the Analysis of the Laplacian of the Electron Density. *Inorg. Chem.* **1994**, *33*, 2115−2121.
(53) Bytheway, I.; Gillespie, R. J.; Tang, T.-H.; Bader, R. F. W. Core Distorsions and Geometries of the Difluorides and Dihydrides of Ca, Sr and Ba. *Inorg. Chem.* **1995**, *34*, 2407−2414.
(54) Gillespie, R. J.; Bytheway, I.; Tang, R. T-H.; Bader, R. F. W. Geometry of the Fluorides, Oxofluorides, Hydrides, and Methanides of Vanadium(V), Chromium (VI), and Molybdenum(VI): Undestanding the Geometry of Non-VSEPR Molecules in Terms of Core Distortion. *Inorg. Chem.* **1996**, *33*, 3954−3963.
(55) Bo, C.; Sarasa, J.-P.; Poblet, J.-M. Laplacian of Charge Density for Binuclear Complexes: Terminal vs Bridging Carbonyls. *J. Phys. Chem.* **1993**, *97*, 6362−6366.
(56) Wang, C.-C.; Wang, Y.; Liu, H.-J.; Chou, K.-J.; Lin, L.-K.; Chan, K.-S. Bond Characterization of Chromium-Fischer Carbene Complexes: A Combined Study of Experiment and Theory. *J. Phys. Chem. A* **1997**, *101*, 8887−8901.
(57) Sierra Alta, A.; Ruette, F. The Laplacian of the Electronic Density at the Valence-Shell Charge Concentration (VSCC): A Comparative Study of Effective Core Potential and Full-Electron Calculations in Mo Compounds. *Int. J. Quantum Chem.* **1996**, *60*, 1015−1026.
(58) Gillespie, R. J.; Popelier, P. L. A. *Chemical Bonding and Molecular Geometry*; Oxford University Press: NY, USA, 2001.
(59) Machi, P.; Sironi, A. Chemical Bonding in transition Metal Carbonyl Clusters: Complementary Analysis of Theoretical and Experimental Electron Densities. *Coord. Chem. Rev.* **2003**, *238*, 383−412.
(60) Cortés-Guzmán, F.; Bader, R. F. W. Complementarity of QTAIM and MO Theory In The Study of Bonding in Donor−Acceptor Complexes. *Coord. Chem. Rev.* **2005**, *249*, 633−662.
(61) Frenking, G.; Sola, M.; Vyboishchikov, S. F. Chemical Bonding in Transition Metal Carbene Complexes. *J. Organomet. Chem.* **2005**, *690*, 6178−6204.
(62) Otero-de-la-Roza, A.; Luaña, V. Topological Characterization of the Electron Density Laplacian in Crystals. The Case of the Group IV Elements. *J. Chem. Theory Comput.* **2010**, *6*, 3761−3779.
(63) MacDougall, P. J.; Hall, M. B.; Bader, R. F. W.; Cheeseman, J. R. Extending the VSEPR model through the properties of the Laplacian of the charge density. *Can. J. Chem.* **1989**, *67*, 1842−1846.
(64) Malcom, N. O. J.; Popelier, P. L. A. The Full Topology of the Laplacian of the Electron Density: Scrutinising a Physical Basis for the VSEPR Model. *Faraday Discuss.* **2003**, *124*, 353−363.
(65) Guillespie, R. J. Fifty Years of the VSEPR Model. *Coord. Chem. Rev.* **2008**, *252*, 1315−1327.
(66) Guillespie, R. J.; Hargitattai, I. *The VSEPR Model of Molecular Geometry*; Dover Pub. Inc: New York, 2012.
(67) Bader, R. F. W.; Johnson, S.; Tang, T. H.; Popelier, P. L. A. The Electron Pair. *J. Phys. Chem.* **1996**, *100*, 15398−15415.
(68) Becke, D.; Edgecombe, K. E. A Simple Measure of Electron Localization in Atomic and Molecular Systems. *J. Chem. Phys.* **1990**, *92*, 5397.
(69) Note that this topological structure does not match that of a mathematical graph. See, for instance: Bollobas, B. *Modern Graph Theory*; Springer: NY, USA, 1998.
(70) Mathematically, the association of CPs with cells was demonstrated by Franks (Franks, J. M. Morse-Smale Flows and Homotopy Theory. *Topology* **1979**, *18*, 199−215) for some particular vector fields (Morse-Smale) and on compact manifolds. The point is that this association is only valid for Morse function (with non-degenerate CPs) compact manifolds.
(71) Matsumoto, Y. *An Introduction to Morse Theory*; Iwanam Series in Modern Mathematics; American Mathematical Society: Providence, RI, USA, 2002; Vol. *208*.
(72) Kotus, J.; Krych M.; Nitecki, Z. *Global Structural Stability of flows on open surfaces*; Memoirs of the American Mathematical Society, no. *261*; American Mathematical Society: Providence, RI, 1982.
(73) Hirsch, M.; Smale, S.; Devaney, R. L. *Differential Equations, Dynamical Systems and An Introduction to Chaos*, 2nd ed.; Elsevier: San Diego, California, USA, 2004.
(74) Berkowitz, M.; Ghosh, S. K.; Parr, R. G. On the Concept of Local Hardness in Chemistry. *J. Am. Chem. Soc.* **1985**, *107*, 6814−6818.
(75) Bone, R. G. A.; Bader, R. F. W. Identifying and Analyzing Intermolecular Bonding Interactions in van der Waals Molecules. *J. Phys. Chem.* **1996**, *100*, 10892−10911.
(76) Deslongchamps, P. *Stereolectronic Effects in Organic Chemistry*; Pergamon Press: Oxford, England, 1983.
(77) Greenwood, N. N.; Earnshaw, A. *Chemistry of Elements*; Pergamon Press: Oxford, England, 1990.
(78) Vydrov, O. A.; Scuseria, G. E. Assessment of a Long-Range Corrected Hybrid Functional. *J. Chem. Phys.* **2006**, *125*, 234109.
(79) Vydrov, O. A.; Scuseria, G. E.; Perdew, J. P. Tests of Functionals for Systems with Fractional Electron Number. *J. Chem. Phys.* **2007**, *126*, 154109.
(80) Zhao, Y.; Truhlar, D. G. Density Functionals with Broad Applicability in Chemistry. *Acc. Chem. Res.* **2008**, *41*, 157−167.
(81) Chai, J.-D.; Head-Gordon, M. Long-range Corrected Hybrid Density Functionals With Damped Atom−Atom Dispersion Corrections. *Phys. Chem. Chem. Phys.* **2008**, *10*, 6615−6620.
(82) Yang, K.; Zheng, J.; Zhao, Y.; Truhlar, D. G. Tests of the RPBE, revPBE, $\tau$-HCTHhyb, $\omega$B97X-D, and MOHLYP Density Functional Approximations and 29 Others Against Representative Databases For Diverse Bond Energies and Barrier Heights In Catalysis. *J. Chem. Phys.* **2010**, *132*, 164117.
(83) Tsipis, A. C. DFT Flavor of Coordination Chemistry. *Coord. Chem. Rev.* **2014**, *272*, 1−29.
(84) Tsipis, A. C. DFT/TDFFT Insights Into the Chemistry, Biochemistry and Photohysics of Copper Coordination Compounds. *RSC Adv.* **2014**, *4*, 32504−32529.
(85) Frisch, M. J.; Trucks, G. W.; Schlegel, H. B.; Scuseria, G. E.; Robb, M. A.; Cheeseman, J. R.; Scalmani, G.; Barone, V.; Mennucci, B.; Petersson, G. A.; et al. *Gaussian 09*, revision B.01 and revision C.01, G09W, revision A.02 SMP; Gaussian, Inc.: Wallingford, CT, 2010.
(86) Dennington, R.; Keith, T.; Millam, J. *GaussView 5.0.8*; Semichem Inc.: Shawnee Mission, KS, 2009.


DOI: 10.1021/jp5055414
*J. Phys. Chem. B* 2015, 119, 1243−1258

(87) Tomasi, J.; Mennucci, B.; Cammi, R. Quantum Mechanical Continuum Solvation Models. *Chem. Rev.* **2005**, *105*, 2999−3093.
(88) Hratchian, P.; Schlegel, H. B. Using Hessian updating to increase the efficiency of a Hessian based predictor-corrector reaction path following method. *J. Chem. Theory Comput.* **2005**, *1*, 61−69.
(89) Fradera, X.; Austen, M. A.; Bader, R. F. W. The Lewis Model and Beyond. *J. Phys. Chem. A* **1999**, *103*, 304−314.
(90) AIM2000 v.2. Biegler-König, F.; Schönbohm, J. Update of the AIM2000-Program for Atoms in Molecules. *J. Comput. Chem.* **2002**, *23*, 1489−1494.
(91) Matito, E.; Silvi, B.; Duran, M.; Solá, M. Electron localization Function At The Correlated Level. *J. Chem. Phys.* **2006**, *125*, 024301.
(92) Johnson, E. R.; Keinan, S.; Mori-Sánchez, P.; Contreras-García, J.; Cohen, A. J.; Yang, W. Revealing Noncovalent Interactions. *J. Am. Chem. Soc.* **2010**, *132*, 6498−6506.
(93) Gabedit 2.4.7: Allouche, A. R. Gabedit—A Graphical User Interface for Computational Chemistry Softwares. *J. Comput. Chem.* **2011**, *32*, 174−182.
(94) Lee, T. J.; Rendell, A. P.; Taylor, P. R. Comparison of the Quadratic Configuration Interaction and Coupled-Cluster Approaches to Electron Correlation Including the Effect of Triple Excitations. *J. Phys. Chem.* **1990**, *94*, 5463−5468.
(95) Bauernschmitt, R.; Ahlrichs, R. Stability Analysis for Solutions of the Closed Shell Kohn-Sham Equation. *J. Chem. Phys.* **1996**, *104*, 9047−9052.
(96) Löwdin, P.-O. Natural Orbitals in the Quantum Theory of Two-Electron Systems. *Phys. Rev.* **1956**, *101*, 1730−1739.
(97) Bader, R. F. W.; Essen, H. The Characterization of Atomic Interactions. *J. Chem. Phys.* **1984**, *80*, 1943−1960.
(98) Bader, R. F. W. A Bond Path: A Universal Indicator of Bonded Interactions. *J. Phys. Chem. A* **1998**, *102*, 7314−7323.
(99) Bader, R. F. W. Bond Paths Are Not Chemical Bonds. *J. Phys. Chem. A* **2009**, *113*, 10391−10396.
(100) Bader, R. F. W.; Nguyen-Dang, T. T.; Tal, Y. Quantum Topology of Molecular Charge Distributions. II. Molecular Structure and its Change. *J. Chem. Phys.* **1979**, *70*, 4316−4329.
(101) Krokidis, X.; Noury, S.; Silvi, B. Characterization of Elementary Chemical Processes by Catastrophe Theory. *J. Phys. Chem. A* **1997**, *101*, 7277−7282.
(102) Berski, S.; Andrés, J.; Silvi, B.; Domingo, L. R. The Joint Use of Catastrophe Theory and Electron Localization Function to Characterize Molecular Mechanisms. A Density Functional Study of the Diels-Alder Reaction between Ethylene and 1,3-Butadiene. *J. Phys. Chem. A* **2003**, *107*, 6014−6024.
(103) Mbouombouo Ndassa, I.; Silvi, B.; Volatron, F. Understanding Reaction Mechanisms in Organic Chemistry from Catastrophe Theory:Ozone Addition on Benzene. *J. Phys. Chem. A* **2010**, *114*, 12900−12906.
(104) Pearson, R. G.; Songstad, J. Application of the Principle of Hard and Soft Acids and Bases to Organic Chemistry. *J. Am. Chem. Soc.* **1967**, *89*, 1827−1836.
(105) Macchi, P.; Sironi, A. Interactions Involving Metals: From Chemical Categories to QTAIM and Backwards. In *The Quantum Theory of Atoms in Molecules*; Matta, C. F., Boyd, R., Eds.; Wiley-VCH: Weinheim, 2007; pp 345−374.


DOI: 10.1021/jp5055414
*J. Phys. Chem. B* 2015, 119, 1243−1258